PULLOUT OF A NEO-HOOKEAN FIBER EMBEDDED IN A GENERALIZED NEO-HOOKEAN MATRIX

A Thesis

by

PRATYUSA KAR

Submitted to the Graduate and Professional School of
Texas A&M University
in partial fulfillment of the requirements for the degree of

MASTER OF SCIENCE

Chair of Committee,	Chandler Benjamin
Co-Chair of Committee,	Alan Freed
Committee Members,	Anastasia Muliana
	Emily Pentzer
Head of Department,	Guillermo Aguilar

December 2021

Major Subject: Mechanical Engineering

ABSTRACT

In this work, the mechanical behavior of a neo-Hookean fiber embedded in a generalized neo-Hookean matrix, is studied. The fiber is subjected to an axial pullout displacement. Based on past pullout experimental conditions, three different boundary value problems are studied here. Extensive stress analysis is conducted using Comsol, as the finite element software. Past literature considered the pullout phenomenon of stiff fibers. In this work, both soft and stiff fibers are studied and the deformation and the shear stress distributions are analyzed with varying shear modulus of the fiber. It is observed that, for a soft fiber, most of the deformation is localized at the top extended portion of the fiber with negligible deformation in the matrix region. Whereas, for a stiff fiber, there is significant deformation in the matrix. As a result, the shear stress is found to be increasing with an increase in the stiffness of the fiber. Further discussion is made on the effect of embedded length on the shear stress distribution. Additionally, some parametric studies are conducted by varying the material and the geometric parameters to observe the crucial effect on the shear stress distribution. In most of the past pullout tests conducted, the pullout force was studied with respect to the applied displacement. A similar analysis is done in this study which will aid in future experiments to be conducted. Moreover, this study can be extended to an analytical formulation of the debond forces arising due to the axial pullout of the same fiber-matrix system.

DEDICATION

This work is dedicated to my parents, Prasun Kar and Mita Kar, for instilling in me an admiration for science and technology, encouraging me in all my academic pursuits, and ensuring good mental and physical health. Without their sustained support in all my decisions and numerous sacrifices, this wouldn't have been possible.

ACKNOWLEDGMENTS

I would like to acknowledge my committee chair Dr. Chandler Benjamin and doctoral candidate, Manoj Myneni, for their guidance through the course of this research. Additionally, I would like to thank my co-chair Dr. Alan Freed, my committee members, Dr. Anastasia Muliana, and Dr. Emily Pentzer for their assistance in computational and theoretical understanding of the work.

I would also like to thank Dr. K.R. Rajagopal for his insights on the research conducted here. A special thanks to my research group whose frequent feedback on the work was significant for the success of this research.

CONTRIBUTORS AND FUNDING SOURCES

Contributors

This work was supported by a thesis committee consisting of Dr. Chandler Benjamin and Manoj Myneni of the Department of Mechanical Engineering.

Funding Sources

Graduate study was supported by TEES - Texas A&M Engineering Experiment Station.

TABLE OF CONTENTS

Page

LIST OF FIGURES

FIGURE Page

1. INTRODUCTION AND LITERATURE REVIEW

1.1 Thesis Introduction

In this work, the deformation and the stress experienced by a fiber-matrix system are studied during a pullout phenomenon. The boundary value problem considered here consists of a fiber in the form of a cylinder of radius a, embedded in a cylinder of radius r, made of the matrix material and is displaced along its axis (see figure 2.1). The dependence of the deformation and the stress on the axial displacement of the fiber, the material and the geometric parameters is considered here. Based on the existing fiber pullout experiments, the configuration studied here has a cylindrical fiber-matrix system with the fiber, partially embedded in the matrix and is extended at the end where it is pulled out [1, 2, 3] (see figure 2.1). This configuration is then studied for two boundary conditions. The first study is done by keeping the bottom of the geometry fixed and pulling the fiber from the top [4, 5, 6, 7] (see figure 2.1-b). In the second study, the outer cylindrical surface of the matrix is fixed and the fiber is pulled from the top [8] (see figure 2.1-c). Further, the study is broadened to a case where the fiber is extended out of the matrix at both ends, keeping the matrix cylindrical surface fixed. We will call this geometry; a fully embedded fiber in the matrix (see figure 2.1-a).

The pullout phenomenon of a fiber-reinforced composites and polymers has been studied in the past and the stresses required to debond the fiber-matrix interface and to pull out a fiber were examined. Most of the previous research focused on a pullout phenomenon in the fiber-matrix systems, where the fiber is much stiffer than the matrix material. For example, the pullout phenomenon was studied for brass-plated steel wire chords, aluminum, glass fibers embedded in a matrix of rubber or concrete composites exhibiting linearized elastic properties (see [9, 5, 4, 10]). Several computational studies also examined the stress distribution in the fiber-matrix system during a pullout experiment wherein the fiber was modeled as a linearized elastic material. Recently, analytical and experimental studies are being conducted with fibers made from polymers (see [11, 8, 12, 13, 7]),

whose stiffness is comparable to that of the matrix. In order to study the behavior of the fibers made of soft materials, that behave nonlinearly, a non-linear material model is used. Here, the generalized neo-Hookean material model for the fiber-matrix system is considered to study the fiber pullout phenomenon with fiber stiffness comparable to that of the matrix. In most of the past work, the shear stress distribution along the fiber-matrix interface is studied, considering stiff fibers embedded in composites [6, 14, 2, 3]. In this work, the interfacial shear stress distribution will be studied for both soft and stiff fibers embedded in a matrix. Additionally, the differences, if any, in the interfacial shear stress distribution will be observed for a soft vs. a stiff fiber system.

The pullout phenomenon, in general, is a result of the debonding occurring at the fiber-matrix interface. The debonding of the fiber at the interface has been studied using different theoretical approaches [1, 2]. A strength-based approach assumed a shear lag model of fiber and matrix, where the interfacial debonding initiates when maximum interfacial shear stress exceeds interfacial shear strength [2, 3, 15, 16]. The pullout phenomenon in a fiber-reinforced composite or polymer is accompanied by a stress transfer from the fiber to the surrounding matrix by the interfacial shear stress [8, 17, 2, 15, 16]. Additionally, the literature concluded that the initial debonding of a stiff fiber embedded in composite or polymer matrix occurs at a point of high stress concentration, which then grows, followed by a complete breaking by the pullout load on reaching the critical shear stress. Hence, the focus is laid on studying the distribution of the interfacial shear stress along the fiber length in this work. The stress analysis conducted here for a soft fiber-matrix system gives insights into the stress distribution, which can be used to determine the localized stress concentrated regions, to further study the debond strength in the future. In recent years, studies based on these analytical models have been accompanied by finite element simulations implementing an interfacial model to capture the pullout behavior and calculate the interfacial stress distributions [16]. In such simulations, the fiber-matrix interface was considered as a thin elastic layer with distinct interfacial behavior with FE mesh density high at the corners of the interface [18, 19]. The effect of embedded length and the matrix radius on the interfacial behavior was analyzed henceforth. In this work, a finite element analysis is performed on a nonlinear material model

with a similar interfacial region of high mesh density and linearly varying parameters indicating a smooth transition from the fiber to the matrix region. In addition to the stress distribution and deformation, it is important to note the force required to pull out a fiber embedded in a matrix. Both theoretical studies and fiber pullout experiments have been conducted to assess this force for stiff fiber-composite/polymer matrix systems. The single fiber pullout test was used to directly examine the fiber-matrix interfacial shear stress which was determined from the measured debond/pullout force and the measured fiber embedded length [20, 21, 5, 19]. Additionally, the applied load was measured during progressive failure to generate a load-displacement curve [21]. Single pullout tests were also performed to assess the effect of geometrical and material parameters on the pull-out phenomenon at the fiber-matrix interface [4, 22]. The experimental results were found to show a behavior where pullout load is a function of the embedded length and displacement [5]. In this study, similar pullout force versus displacement curves is analyzed for the soft fiber-matrix system considered, which will be used in conjunction with future pullout tests on soft fiber and matrix.

Primarily, in this work, the boundary value problem for the fiber pullout is solved, where the pullout force is analyzed, which is required for different pullout displacements applied at the fiber end. The non-uniform behavior of the shear stress at the interface is noted along with an extensive stress analysis for the entire system. In the above-mentioned literature, the stress field arising in the fiber pullout phenomenon is analyzed within the framework of the linear theory of elasticity [6]. The generalized neo-Hookean material model for the fiber-matrix system is considered to study the nonlinear behavior of the fiber-matrix interface during a fiber pullout phenomenon.

The organization of the work is as follows: The layout is initiated with the preliminaries of the basic kinematics. The power law neo-Hookean model in terms of stored energy is introduced and the constitutive relations are formed. Following this, the boundary value problems to be studied, are introduced, and the equilibrium equations governing the problems are documented. Extensive stress analysis is performed with different parameters for the problems. After having some significant results, discussions are made on the mechanical behavior of the fiber-matrix system. Finally, a general conclusion will be drawn from the observation and discussions on the behavior of the

boundary value problems.

1.2 Literature Review

1.2.1 Analytical Fiber Pullout Studies

Pullout studies were done mostly by using either of the two theories; a stress transfer theory at the fiber-matrix interface or the debonding theory using the Griffith criteria of fracture. The stress transfer theory typically assumed that the stress transfers from the fiber to the matrix on loading by interfacial shear stress. After the initial debond, the debond stress increases with an increasing debond length. The interfacial debonding initiates when max interfacial shear stress exceeds interfacial shear strength of the interface [6]. According to the Griffith theory, for debonding to occur; the energy supplied by the loading device as the fiber is pulled out must be greater than the energy required to fracture the fiber-matrix interface and increase in the strain energy of the matrix [9].

Stang et al. [23] used both stress and fracture energy approach to compare the two approaches to study the debonding at the interface of fiber and matrix composites due to a pullout of the fiber. The same model is used for both approaches. It was observed that the stress approach was dependent on the critical shear stress value, which is not a material parameter, rather measured from a pullout test, which solely was governed by the type of analysis being performed. However, the fracture energy approach was derived by solutions for the compliance and hence was not governed by refinement of analysis. Fracture criterion identified two uncoupled parameters describing adhesive bond and friction, whereas the stress approach gave solutions that coupled the bond and the friction parameter, giving better insights about the interfacial behavior since the maximum pullout load and stability of the pullout process were seen to depend on the frictional contribution of the interface.

In 1981, Gent assessed the force required to pull out a fiber using Griffith criteria, wherein, linear elasticity theory was demonstrated [9]. The matrix material was rubber and the fiber was assumed to be steel, glass or other high modulus fibers. It was shown that the fiber debonds when the energy released is greater than the energy required for debonding for the crack to propagate.

Using the Griffith theory, the pullout energy is greater than the energy required to fracture the interface and an increase in strain energy of the matrix for the debonding to take place. Pullout force was found to be a function of geometry, Young's Modulus and interfacial bond strength. Inferred value of the interfacial bond strength is compared with experimentally found out bond strength. In pullout tests, a failure is induced and the maximum tensile force for the failure is recorded. The slope of the Pullout force vs displacement curve gave the values of Young's Modulus. Analytically, the pullout force increases with an increase in the Young's Modulus. The dependence of the pullout force with the geometrical parameters like the fiber diameter, the height of the specimen etc. were found in accordance with the experiments conducted. A similar parametric study is conducted in this work, with both soft and stiff fiber, where the dependence of the pullout force with respect to the geometrical parameters will be thoroughly analyzed. These analytical solutions can be validated with pullout experiments to be conducted in the future.

The strength of fiber-reinforced composites is dependent on interfacial properties. In order to study the interfacial strength, Yue [24] analyzed the pullout phenomenon with a strength-based approach according to which the debonding due to the pullout phenomenon occurs when shear stress reaches critical shear stress. Hence in this study, the focus will be laid on studying the stress distribution. In this literature, the effect of the shear modulus ratio was studied and it was observed that for less stiff fiber, interfacial shear stress changes drastically along the fiber, whereas for a stiffer fiber, the interfacial shear stress does not change drastically. Also, it was noted that the interfacial shear strength concentration exists at the embedded end of the fiber. Also, the shear stress with different fiber thicknesses was analyzed. Similar parametric studies with different shear modulus ratios and different fiber thicknesses are conducted in this work.

Hsueh studied the interfacial properties of composites during a fiber pullout where the solution of initial debonding due to an applied axial tensile stress on the fiber was established, and the relation between the debond stress and debond length was developed using a shear lag model of fiber at the center of a coaxial cylindrical matrix [6]. According to this study, the initiation of the debonding due to the pullout force occurs at the surface, where the fiber enters the matrix since the

shear stress was found to be maximum at that location. Further, the initial debond stress or the bond strength was independent of the fiber length and it was observed that a fiber strength higher than this debond stress is required to initiate the debonding. Additionally, the paper discussed a Poisson contraction of the fiber in the radial direction during the fiber pullout, resulting in a reduction of the compressive stress at the interface.

Following this, another study was performed with a non-constant interfacial bond strength and the axial displacement of the fiber during the pullout was found to be linear with the applied stress [14]. The interface remained bonded when this applied stress was lower than the initial non-constant debond stress. However, these studies did not consider the composite matrix having residual radial and axial stresses. This was addressed in 1990 where the applied stress required to debond the interface also depended on the residual axial stresses but not strongly on the residual radial stresses [2]. In this case, the interface required a strain continuity which led to an axial mismatch strain. This axial mismatch strain induced the interfacial shear stress. It was found that when this interfacial shear stress induced by the axial mismatch strain and the one by the axial applied stress are in the same direction, the axial mismatch strain facilitates the debonding during the pullout [2].

The pullout studies were extended for an improved analysis for the bonded interfaces, where extensive stress analysis was performed for different geometric parameters of the fiber and the matrix with fiber subjected to a pullout axial stress. The stress distribution in a sufficiently long fiber reached a steady state at locations away from the embedded fiber ends with zero interfacial shear stress. On the other hand, the radial stresses were shown to be independent of the radial and axial coordinates at a steady state. However, for a short fiber, the axial stress distribution along the fiber length was more linear, with maximum interfacial shear stress at the corner of the fiber-matrix interface. Conclusions were made on stress transfer and load transfer from fiber to the matrix, owing to which, an occurrence of second maximum interfacial shear stress was noted.

The concept of a relationship between the bond shear stress and the local slip at the fiber-matrix interface was first introduced in 1991 by Naaman et, al. [25]. In this study, a pullout curve was

predicted by assuming a bond-slip relationship which was validated from an experiment pullout curve. This relationship was considered as the constitutive property of the fiber-matrix interface. A pullout test was performed where the fiber, embedded in a cementitious body, was subjected to a tensile force at the tip. A monotonic increase in the value of the applied force was accompanied by a displacement of the fiber tip leading to progressive debonding along the interface. A dynamic mechanism was observed on reaching the embedded end of the fiber. Both the free end and the embedded end witnessed significant displacement.

1.2.2 Experimental Fiber Pullout Studies

Experiments were conducted on a single fiber pullout to examine the mechanical properties, the interfacial stress and the dependencies of the mechanical and geometrical parameters on the fiber-matrix system during the pullout phenomenon. One such experiment was performed to examine the Kevlar fiber epoxy matrix interface bond strength. A nonlinear curve for pullout force vs embedded length was observed. Pullout force was found to be constant with higher embedded length [20]. In 1993, Marotzke performed a single pullout test and analyzed the stress field arising due to the pullout [15]. Two types of elastic fibers embedded in a polycarbonate matrix with a fixed length to diameter ratio were considered. Stress distributions were analyzed as the solutions of a boundary value problem using the finite element method. It was observed that the stress near the fiber is inhomogeneous and there exists high shear and radial stress concentration at the fiber ends highly dependent on the axial stiffness ratio of the fiber and the matrix.

Of many such experimental studies, Gent's study was carried out of debonding and fiber rupture in model composites. A single glass rod (fiber) was embedded in the center of a long silicone rubber matrix. Strains in the matrix near the fiber were measured as the specimen was slowly stretched or pulled out. Pullout forces, strain distributions and debonded lengths were compared with those predicted from fracture energy criterion during debonding [26]. In this study it was concluded the interface between the two materials was smooth which was governed by the observation of an approximate constant friction force between the rubber and the glass. Another mechanical experiment involved fibers embedded in an elastic resin. While the rubber became de-

tached from the base of the rod, a large cavity was formed due to an internal rupture of the rubber under the rod which occurred when the local triaxial tension reached close to Young's modulus of the rubber [27]. The cavitation phenomenon was followed by a debond propagation beginning at the embedded end, resulting in the complete pullout of the fiber. Pullout force was computationally calculated and experimentally measured based on simple fracture mechanics with elastic compliance to establish the consistency of the results. A relation between the pullout force and the displacement was obtained where the force increased linearly with the applied displacement and reaches a peak. The peak force was termed as the critical force, beyond which the force value dropped to a magnitude which was termed as the pullout force.

In most of the experiments, glass rods, stainless steel, kevlar or carbon rods were considered as fibers, however, one experiment was performed with polymer fiber reinforced in hydrogel composites. Interfacial adhesion was determined for different grafting conditions using a fiber pullout test [8]. In this experiment, the fiber-matrix system was held from the circumference and pullout load was applied on the top.

1.2.3 Literature on generalized neo-Hookean material

In recent years, there has been a considerable amount of interest in the study of motions of nonlinear elastic materials. Soft fibers and matrices undergo large deformations and hence exhibit nonlinear elasticity. Such deformations are not general or universal and therefore, need to be studied with the help of specific nonlinear constitutive theories. Considering the power-law exponent as unity, this model reduces to a classical neo-Hookean model which is used in modeling rubber-like solids. Moreover, in plane-strain problems, the equations lose ellipticity for values of power-law exponent less than or equal to half; assisting in interesting qualitative analysis and leading to interesting physical phenomena being observed experimentally. Furthermore, the model takes care of the hardening and softening behavior of materials, exhibiting shear softening for values of exponent (parameter n) between one half and unity and displays shear hardening behavior for values above unity. The parameter b governs the magnitude of this hardening and softening.

The generalized power-law neo-Hookean model was first used in 1977 by Knowles [28] to

study the finite anti-plane shear field near a crack tip. In 1992 Rajagopal and Tao [29] studied the inhomogeneous deformations in a wedge of a generalized neo-Hookean material. They found solutions that have a boundary layer structure. The solution is inhomogeneous adjacent to the boundary and homogeneous in the core region. Further, they observed a bounded pressure field associated with the solutions. In the same year, Zhang and Rajagopal [30] studied inhomogeneous twisting of a slab of a generalized neo-Hookean material about distinct axes allowing discontinuous deformations gradients. They found that the equations admit solutions for which the locus of the centers of rotation is piecewise continuously differentiable for certain values of parameters. Researches were conducted to study the possibility of circular shearing and torsion in power-law neo-Hookean materials. (see Rajagopal, et al. [31]). Explicit exact solutions were established for special values of the power-law exponent. Considering the effect of torsion, expressions were obtained for traction on boundaries and for the moment necessary to incite the deformation. Even unsteady inhomogeneous motions were studied using neo-Hookean models. One such study was conducted by Rajagopal in 2002 [32] to determine explicit new exact solutions for unsteady inhomogeneous motions of a neo-Hookean solid.

The fiber reinforced soft compounds were studied as many boundary value problems over the years. Recently, in 2019, the motion of composite cylindrical annulus made of generalized neo-Hookean elastic solids subjected to periodic shear on the inner boundary was investigated as a boundary value problem (see Benjamin, et al. [33]). Here stress and strain boundary layers were introduced. A stress boundary layer was observed to form in the thick-walled cylinders for both strain hardening and strain softening materials. Strain boundary layers were introduced in thick-walled cylinders for strain softening conditions. The norm of the strain has a large gradient in a narrow region adjacent to the boundaries and a relatively uniform strain outside the narrow region.

From the literature review, few key points were taken into consideration based on which the work proceeded. Most of the literature considered stiff fibers in the past with few cases of a polymer matrix. In this study along with the stiff fibers, fibers with shear modulus comparable to that of the matrix are studied. Based on past literature, the generalized neo-Hookean material model is

the most suitable model to represent the nonlinear behavior of soft fiber and matrix systems. It is significant to note the interfacial shear stress distribution in this work along with the pullout force distribution with applied pullout displacement. Further, the boundary conditions for the problems were taken with reference to the boundary conditions applied in the experiments in the literature. In most cases, the matrix was held along the circumference of the matrix or held from the bottom. Similar boundaries are considered in the work here. Additionally, the effect of the geometric properties and the material properties are studied here.

2. PRELIMINARIES AND PROBLEM DESCRIPTION

2.1 Preliminary Theory

Let **x** denote the current position of a particle in a deformed solid body and let **X** denote the position of a particle in the reference configuration. The displacement of a particle is defined as,

$$\mathbf{u} = \mathbf{x} - \mathbf{X}, \tag{2.1}$$

The deformation gradient is defined by,

$$\mathbf{F} = \frac{\partial \mathbf{x}(\mathbf{X}, \mathbf{t})}{\partial \mathbf{X}}. \tag{2.2}$$

It then follows from the definition of the displacement and the deformation gradient that,

$$\mathbf{F} = \frac{\partial \mathbf{u}}{\partial \mathbf{X}} + \mathbf{I}. \tag{2.3}$$

The right and left Cauchy-Green tensors are defined as,

$$\mathbf{B} = \mathbf{F}\mathbf{F}^{\mathbf{T}}, \quad \mathbf{C} = \mathbf{F}^{\mathbf{T}}\mathbf{F}. \tag{2.4}$$

Let W be the stored energy function associated with an isotropic, homogeneous, compressible Green-elastic material. W is a function of the following form

$$W = W(I_1, I_2, I_3) \tag{2.5}$$

where I_1, I_2, I_3 are the principal invariants of **B** given by

$$I_1 = tr(\mathbf{B}), \quad I_2 = \frac{1}{2}\left[(tr(\mathbf{B}))^2 - tr(\mathbf{B}^2)\right], \quad I_3 = \det(\mathbf{B}). \tag{2.6}$$

The Cauchy stress for the material is given by,

$$\mathbf{T} = \Phi_0 \mathbf{I} + \Phi_1 \mathbf{B} + \Phi_2 \mathbf{B^{-1}}, \tag{2.7}$$

where,

$$\Phi_0 = I_3^{-1/2} \left(I_2 \frac{\partial W}{\partial I_2} + I_3 \frac{\partial W}{\partial I_3} \right), \quad \Phi_1 = 2 I_3^{-1/2} \frac{\partial W}{\partial I_1}, \quad \Phi_2 = -2 I_3^{1/2} \frac{\partial W}{\partial I_2}, \tag{2.8}$$

The first Piola-Kirchoff stress, (**P**), is related to the Cauchy, (**T**) stress by,

$$\mathbf{P} = \det(\mathbf{F}) \mathbf{T} \mathbf{F}^{-\mathbf{T}} \tag{2.9}$$

The Green-St.Venant strain $\mathbf{E}$ is given by:

$$\mathbf{E} = \frac{1}{2}(\mathbf{C} - \mathbf{I}) \tag{2.10}$$

The norm of strain tensors is given by:

$$||\mathbf{E}|| = (tr(\mathbf{E}^T \mathbf{E}))^{1/2} \tag{2.11}$$

2.2 Compressible generalized neo-Hookean material

A stored energy function of the following form is assumed for the fiber and the matrix,

$$W = \kappa (I_3^{1/2} - 1)^2 + \frac{\mu}{2b} \left[1 + \frac{b}{n} (\overline{I}_1 - 3) \right]^n. \tag{2.12}$$

where $\overline{I}_1 = J^{-2/3} I_1 = I_3^{-1/3} I_1$ and κ is the bulk modulus and $J = \det(\mathbf{F}) = I_3^{1/2}$. When the material is incompressible ($I_3 = 1$), this stored energy corresponds to that of a generalized neo-

Hookean material. This stored energy reduces to the classical neoHookean case when the material is incompressible and $n = 1$. Most polymeric materials are often modeled as incompressible materials. Slight compressibility ($\kappa/\mu = 100$) is introduced to aid the computational analysis. The partial derivatives with respect to I_1 and I_3 become,

$$\frac{\partial W}{\partial I_1} = \frac{1}{2}\frac{\mu}{I_3^{1/3}}\left[1 + \frac{b}{n}\left(\frac{I_1}{I_3^{1/3}} - 3\right)\right]^{n-1} \tag{2.13a}$$

$$\frac{\partial W}{\partial I_3} = \kappa\left(1 - I_3^{-1/2}\right) + \frac{\mu}{6}\frac{I_1}{I_3^{4/3}}\left[1 + \frac{b}{n}\left(\frac{I_1}{I_3^{1/3}} - 3\right)\right]^{n-1} \tag{2.13b}$$

where,

$$\Phi_0 = \kappa\left(\sqrt{I_3} - 1\right) + \frac{\mu}{6}\frac{I_1}{(I_3)^{5/6}}\left[1 + \frac{b}{n}\left(\frac{I_1}{\sqrt{I_3}} - 3\right)\right]^{n-1}, \tag{2.14}$$

and,

$$\Phi_1 = \frac{\mu}{\sqrt{I_3}}\left[1 + \frac{b}{n}\left(\frac{I_1}{\sqrt{I_3}} - 3\right)\right]^{n-1}. \tag{2.15}$$

Given the strain energy has no dependence on the second invariant I_2 the Cauchy stress tensor simplifies to,

$$\mathbf{T} = \Phi_o\mathbf{I} + \Phi_1\mathbf{B}, \tag{2.16}$$

The first Piola-Kirchhoff stress becomes,

$$\mathbf{P} = \overline{\Phi}_o\mathbf{F}^{-\mathbf{T}} + \overline{\Phi}_1\mathbf{F}. \tag{2.17}$$

where $\overline{\Phi}_o = \sqrt{I_3}\Phi_o$ and $\overline{\Phi}_1 = \sqrt{I_3}\Phi_1$

2.3 Boundary Value Problem Description

Consider a cylindrical annulus of outer radius $\hat{R}$ and inner radius a, which is referred to as the "matrix". Let a fiber, which is a cylinder of radius a , be embedded into the annulus with its axis coinciding with the axis of the cylindrical annulus. A perfect bonding at the fiber-matrix interface is assumed, i.e. a displacement continuity at the interface is considered. Let the top surface of the fiber be displaced in the axial direction. This problem mimics the pull-out of a fiber from the matrix. The geometries of the three boundary value problems considered in this work are shown in figure 2.1.

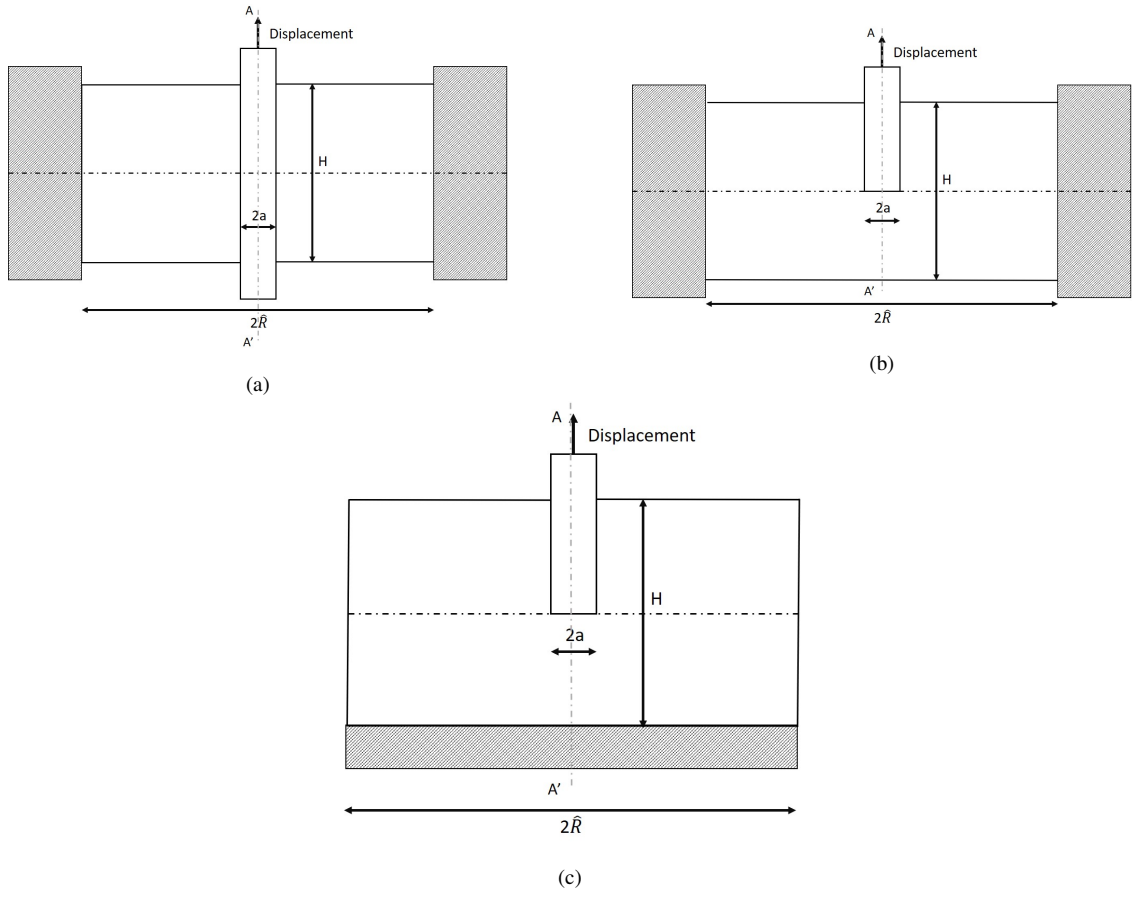

Figure 2.1: (a) Fiber fully embedded in the matrix material with fixed wall, (b) Fiber partially embedded in the matrix material with fixed wall, (c) Fiber partially embedded in the matrix with fixed bottom

For the three boundary value problems considered here, the constitutive relation assumed is given by (2.16) for the matrix, and the values of n, b, μ and κ are varied. Fiber, on the other hand, is modeled using $n = 1$ and $b = 1$, and μ and κ are varied. At the fiber-matrix interface, the parameters n, b, μ, κ vary linearly over a small region from the fiber values to the matrix values.

For the first boundary value problem, the fiber runs through the full length of the matrix and extends beyond the matrix as shown in figure 2.1a. The length of the matrix is given by H. Let the top and bottom surfaces of the matrix at $Z = 0$ and $Z = H$ be traction-free for $a \leq R \leq \hat{R}$ for the matrix (where the bottom surface of the matrix is assumed to coincide with the plane $z = 0$). The surface of the fiber that extends beyond the length of the matrix at $R = a$ is assumed to be traction-free, i.e. $\mathbf{T}.\mathbf{n} = \mathbf{0}$ at $R = \pm a$ for $Z \geq H$ and $Z \leq 0$. The outer surface of the matrix is fixed in all directions i.e. $u_R(R = \hat{R}) = 0$ and $u_Z(R = \hat{R}) = 0$.

For the second boundary value problem, the fiber is partially embedded in the matrix material extending until half the length of the matrix as shown in figure 2.1b. Boundary conditions of this problem remain similar to the previous problem. In the third boundary value problem, the bottom surface of the matrix is fixed in all directions, while the outer surface at $R = \hat{R}$ remains traction-free, as shown in figure 2.1c.

Due to the geometry, the material and the loading conditions, these two boundary value problems can be modeled as axisymmetric problems with the z-axis coinciding with the axis of the cylinder.

2.3.1 Equations of Motion

For the fully and the partially embedded fiber problems, the following displacement field is considered.

$$\mathbf{u} = u_R(R, Z)\hat{e}_R + u_Z(R, Z)\hat{e}_Z, \tag{2.18}$$

The following non-dimensionalization for the variables is taken into account.

$$u_R^* = \frac{u_R}{\hat{R}}, \quad u_Z^* = \frac{u_Z}{H}, \quad R^* = \frac{R}{\hat{R}}, \quad Z^* = \frac{Z}{H} \tag{2.19a}$$

$$\frac{\partial u_R}{\partial R} = \frac{\partial u_R^*}{\partial R^*}, \quad \frac{\partial u_Z}{\partial Z} = \frac{\partial u_Z^*}{\partial Z^*}, \quad \frac{\partial u_R}{\partial Z} = \frac{\hat{R}}{H}\frac{\partial u_R^*}{\partial Z^*}, \quad \frac{\partial u_Z}{\partial R} = \frac{H}{\hat{R}}\frac{\partial u_Z^*}{\partial R^*}, \tag{2.19b}$$

$$\Phi_0^* = \frac{\Phi_0}{\mu_m} = \frac{\kappa}{\mu_m}\left(\sqrt{I_3} - 1\right) + \frac{\mu}{\mu_m}\frac{1}{6}\frac{I_1}{(I_3)^{5/6}}\left[1 + \frac{b}{n}\left(\frac{I_1}{\sqrt{I_3}} - 3\right)\right]^{n-1}, \tag{2.19c}$$

$$\Phi_1^* = \frac{\Phi_1}{\mu_m} = \frac{\mu}{\mu_m}\frac{1}{\sqrt{I_3}}\left[1 + \frac{b}{n}\left(\frac{I_1}{\sqrt{I_3}} - 3\right)\right]^{n-1}, \tag{2.19d}$$

$$\tag{2.19e}$$

The displacement gradient is given by[1],

$$\nabla \mathbf{u} = \begin{bmatrix} \frac{\partial u_R^*}{\partial R^*} & 0 & \frac{\hat{R}}{H}\frac{\partial u_R^*}{\partial Z^*} \\ 0 & \frac{u_R^*}{R^*} & 0 \\ \frac{H}{\hat{R}}\frac{\partial u_Z^*}{\partial R^*} & 0 & \frac{\partial u_Z^*}{\partial Z^*} \end{bmatrix}. \tag{2.20}$$

The deformation gradient and the inverse transpose of the deformation gradient are given by,

$$\mathbf{F} = \begin{bmatrix} 1 + \frac{\partial u_R^*}{\partial R^*} & 0 & \frac{\hat{R}}{H}\frac{\partial u_R^*}{\partial Z^*} \\ 0 & 1 + \frac{u_R^*}{R^*} & 0 \\ \frac{H}{\hat{R}}\frac{\partial u_Z^*}{\partial R^*} & 0 & 1 + \frac{\partial u_Z^*}{\partial Z^*} \end{bmatrix}, \tag{2.21}$$

$$\mathbf{F}^{-\mathbf{T}} = \xi^{-1}\begin{bmatrix} -\left(1 + \frac{\partial u_Z^*}{\partial Z^*}\right) & 0 & \frac{H}{\hat{R}}\frac{\partial u_Z^*}{\partial R^*} \\ 0 & \frac{\xi}{1 + \frac{u_R^*}{R^*}} & 0 \\ \frac{\hat{R}}{H}\frac{\partial u_R^*}{\partial Z^*} & 0 & -\left(1 + \frac{\partial u_R^*}{\partial R^*}\right) \end{bmatrix}, \tag{2.22}$$

[1]the notation $(\cdot)(R, Z)$ is suppressed for notational convenience after the introduction of the given displacement vector.

where,

$$\xi = \frac{\partial u_Z^*}{\partial R^*}\frac{\partial u_R^*}{\partial Z^*} - \left(1 + \frac{\partial u_R^*}{\partial R^*}\right)\left(1 + \frac{\partial u_Z^*}{\partial Z}\right), \tag{2.23}$$

The left Cauchy-Green deformation tensor becomes,

$$\mathbf{B} = \begin{bmatrix} \left(1 + \frac{\partial u_R^*}{\partial R^*}\right)^2 + \left(\frac{\hat{R}}{H}\frac{\partial u_R^*}{\partial Z^*}\right)^2 & 0 & \frac{H}{\hat{R}}\frac{\partial u_Z^*}{\partial R^*}\left(1 + \frac{\partial u_R^*}{\partial R^*}\right) + \frac{\hat{R}}{H}\frac{\partial u_R^*}{\partial Z^*}\left(1 + \frac{\partial u_Z^*}{\partial Z^*}\right) \\ 0 & \left(1 + \frac{u_R^*}{R^*}\right)^2 & 0 \\ \frac{H}{\hat{R}}\frac{\partial u_Z^*}{\partial R^*}\left(1 + \frac{\partial u_R^*}{\partial R^*}\right) + \frac{\hat{R}}{H}\frac{\partial u_R^*}{\partial Z^*}\left(1 + \frac{\partial u_Z^*}{\partial Z^*}\right) & 0 & \left(1 + \frac{\partial u_Z^*}{\partial Z^*}\right)^2 + \left(\frac{H}{\hat{R}}\frac{\partial u_Z^*}{\partial R^*}\right)^2 \end{bmatrix}, \tag{2.24}$$

The Cauchy stress tensor is given by equation (2.16),

$$\mathbf{T} = \begin{bmatrix} \Phi_0^* + \Phi_1^*\left[\left(1 + \frac{\partial u_R^*}{\partial R^*}\right)^2 + \left(\frac{\hat{R}}{H}\frac{\partial u_R^*}{\partial Z^*}\right)^2\right] & 0 & \Phi_1^*\left[\frac{H}{\hat{R}}\frac{\partial u_Z^*}{\partial R^*}\left(1 + \frac{\partial u_R^*}{\partial R^*}\right) + \frac{\hat{R}}{H}\frac{\partial u_R^*}{\partial Z^*}\left(1 + \frac{\partial u_Z^*}{\partial Z^*}\right)\right] \\ 0 & \Phi_0^* + \Phi_1^*\left[\left(1 + \frac{u_R^*}{R^*}\right)^2\right] & 0 \\ \Phi_1^*\left[\frac{H}{\hat{R}}\frac{\partial u_Z^*}{\partial R^*}\left(1 + \frac{\partial u_R^*}{\partial R^*}\right) + \frac{\hat{R}}{H}\frac{\partial u_R^*}{\partial z^*}\left(1 + \frac{\partial u_Z^*}{\partial Z^*}\right)\right] & 0 & \Phi_0^* + \Phi_1^*\left[\left(1 + \frac{\partial u_Z^*}{\partial Z^*}\right)^2 + \left(\frac{H}{\hat{R}}\frac{\partial u_Z^*}{\partial R^*}\right)^2\right] \end{bmatrix}, \tag{2.25}$$

From equation (2.17) the components for the first Piola-Kirchoff stress are obtained as,

$$\mathbf{P} = \begin{bmatrix} -\xi^{-1}\overline{\Phi}_o^*\left(1 + \frac{\partial u_Z^*}{\partial Z^*}\right) + \overline{\Phi}_1^*\left(1 + \frac{\partial u_R^*}{\partial R^*}\right) & 0 & \xi^{-1}\overline{\Phi}_o^*\left(\frac{H}{\hat{R}}\frac{\partial u_Z^*}{\partial R^*}\right) + \overline{\Phi}_1^*\left(\frac{\hat{R}}{H}\frac{\partial u_R^*}{\partial Z^*}\right) \\ 0 & \overline{\Phi}_o^*\left(\frac{1}{1 + \frac{u_R^*}{R^*}}\right) + \overline{\Phi}_1^*\left(1 + \frac{u_R^*}{R^*}\right) & 0 \\ \xi^{-1}\overline{\Phi}_o^*\left(\frac{\hat{R}}{H}\frac{\partial u_R^*}{\partial Z^*}\right) + \overline{\Phi}_1^*\left(\frac{H}{\hat{R}}\frac{\partial u_Z^*}{\partial R^*}\right) & 0 & -\xi^{-1}\overline{\Phi}_o^*\left(1 + \frac{\partial u_R^*}{\partial R^*}\right) + \overline{\Phi}_1^*\left(1 + \frac{\partial u_Z^*}{\partial Z^*}\right) \end{bmatrix}, \tag{2.26}$$

The balance of linear momentum, in the absence of body forces, for the special form of the motion

assumed, reduces to,

$$\frac{\partial(R^* P_{RR})}{\partial R^*} + \left(\frac{\hat{R}}{H}\right) \frac{\partial(R^* P_{RZ})}{\partial Z^*} = P_{\Theta\Theta}, \tag{2.27a}$$

$$\frac{\partial(R^* P_{ZR})}{\partial R^*} + \left(\frac{\hat{R}}{H}\right) \frac{\partial(R^* P_{ZZ})}{\partial Z^*} = 0. \tag{2.27b}$$

At the axis of the fiber, a zero shear stress is assumed; $T_{rz} = 0$ and the radial displacement is $u_R = 0$. For the first two problems, the bottom extended portion of the fiber beyond the matrix, the top boundary of the matrix and the bottom boundary of the matrix are traction-free with $\mathbf{P}.\hat{\mathbf{n}} = 0$, where $\hat{\mathbf{n}}$ is the unit outward normal to the surface. The axial and radial displacements at the outer radius of the matrix are prescribed as $u_Z = 0$ and $u_R = 0$. For the third problem, the outer radius of the matrix is traction-free with $\mathbf{P}.\hat{\mathbf{n}} = 0$ and the bottom surface of the matrix is fixed in all directions as $u_Z = 0$ and $u_R = 0$. The top extended portion of the fiber beyond the matrix has axial displacement $u_Z = u_{0T}$. The pullout force at the top of the fiber is calculated as:

$$F_{pullout} = \int_{\Gamma} 2\pi P_{zz} R \, dR \tag{2.28}$$

Figure 2.2 shows the axisymmetric models for the fully and the partially embedded fiber with the boundary conditions.

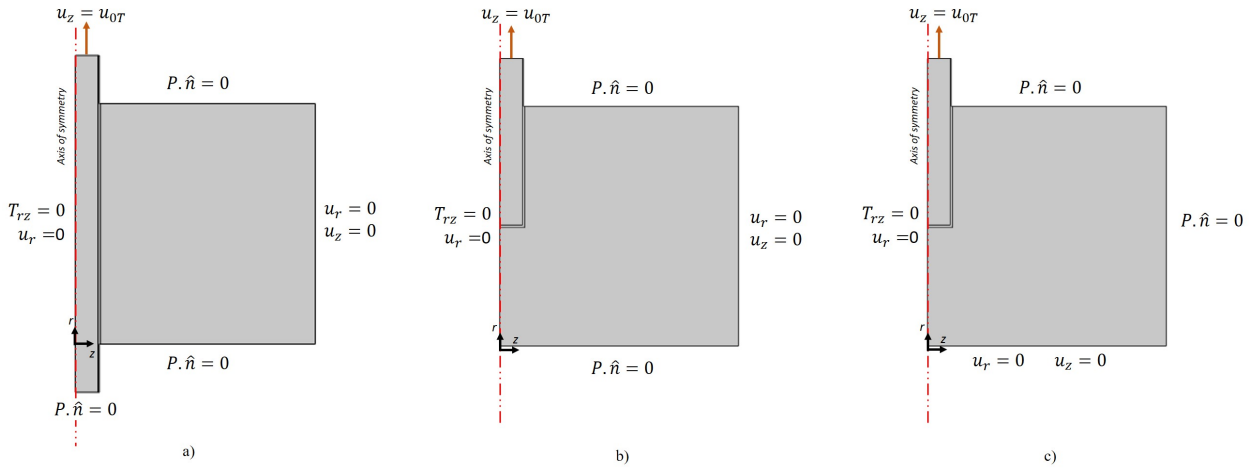

Figure 2.2: Axisymmetric model geometry with boundary conditions. a) Fully Embedded Fiber with fixed wall. b) Partially Embedded Fiber with fixed wall. c) Partially Embedded Fiber with fixed bottom.

Using the above geometry, the finite element analysis is performed to observe the model behavior under the given boundary conditions.

2.3.2 FE Model

The meshed models associated with the three problems are given in figures 2.3a and 2.3b. At the fiber-matrix interface, the material parameters (n, b, μ, K) vary linearly over a small region to capture the smooth transition of these values from the fiber side to the matrix side as shown in 2.3c.

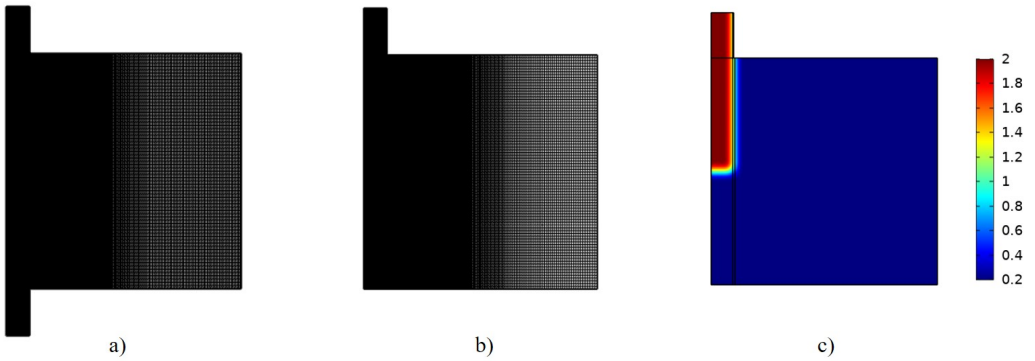

Figure 2.3: a) Meshed model of fully embedded fiber. b) Meshed model of partially embedded fiber. c) Model showing the smooth transition of material parameters varying linearly at the fiber-matrix interface.

The fiber is modeled as a neo-Hookean material. For the matrix, n is varied from 0.6 to 5 with b fixed at 1.

In order to check the dependency of the finite element solution on the mesh size, a mesh convergence study is performed wherein, a coarser and a finer mesh is considered, relative to the mesh that is used in the simulations. The change in the solutions is observed with different mesh sizes.

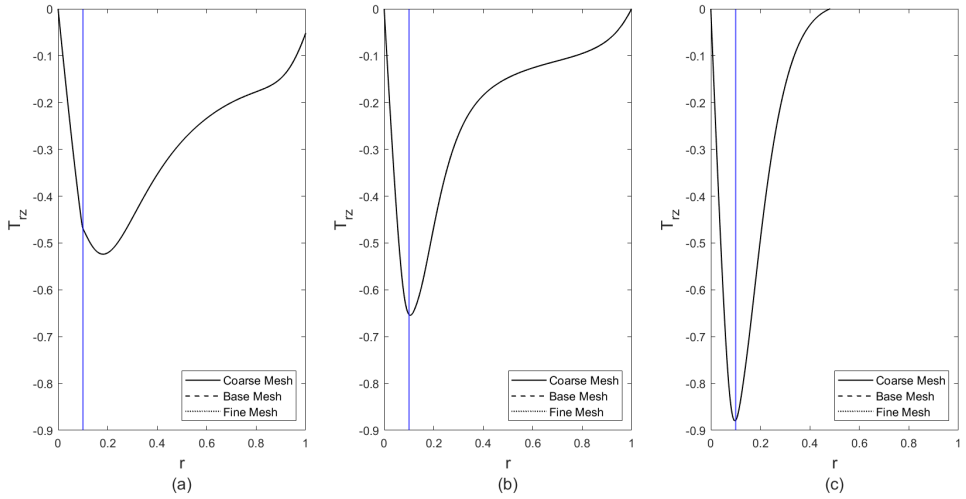

Figure 2.4: Solutions for shear stress for a) Fully Embedded Fiber with fixed outer surface, b) Partially embedded fiber with fixed outer surface, c) Partially embedded fiber with fixed bottom; with different mesh refinements; Overlapping curves for the different mesh size indicating solutions remain same with different mesh. (Blue line shows the fiber-matrix interface).

The stress, being a gradient is the last variable to converge. Hence, the shear stress as a function of the radial distance for different mesh sizes is plotted. As shown in figure 2.4, the solutions do not get altered or affected by the mesh. Therefore, using this mesh, the parametric studies are performed.

3. RESULTS AND DISCUSSION

3.1 Interfacial Shear Stress

In this section, the interfacial shear stress distribution is noted along the fiber length for both soft and a stiff fiber. From figure 3.2, for the fully and the partially embedded fiber systems (embedded length is 0.7 of the total matrix height) and for both the boundary conditions, we observe that, as the fiber becomes stiffer, the interfacial shear stress increases. This can be explained as follows. For soft fibers, the deformation is localized only in the top extended portion of the fiber, whereas for stiff fibers with $(\mu_f : \mu_m = 100 : 1, 200 : 1)$, a larger portion of the matrix deforms, thereby increasing the shear stress along the fiber-matrix interface.

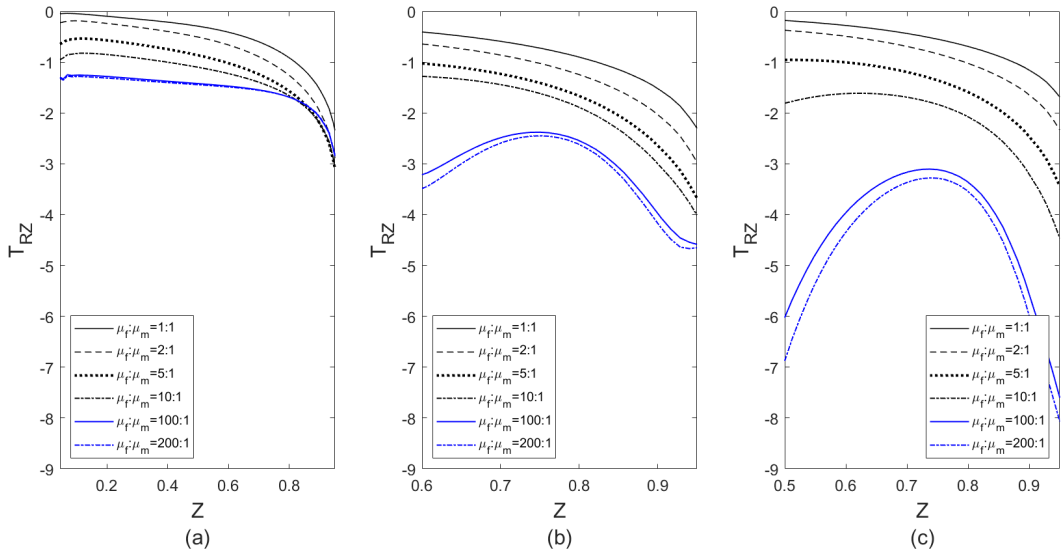

Figure 3.1: Shear stress at the interface in axial direction along the embedded fiber length for a) Fully embedded fiber with fixed outer surface and b) Partially embedded fiber (embedded length is 0.7 times the total matrix height) with fixed outer surface, c) Partially embedded fiber (embedded length is 0.7 times the total matrix height) with fixed bottom; for soft fiber $(\mu_f : \mu_m = 1 : 1, 2 : 1, 5 : 1, 10 : 1)$ and stiff fiber $(\mu_f : \mu_m = 100 : 1, 200 : 1)$ $(n_f = 1, n_m = 0.6, b_f = b_m = 1, u_{0T} = 0.25)$

3.2 Fiber Embedded Length

In this section, further study is done on the interfacial shear stress distribution for the second boundary value problem with varying embedded length. The embedded length is parameterized as a fraction of the total height H of the matrix and the variable used in the analytical model is L_{embed}. Figure 3.1 shows the shear stress distribution along the fiber-matrix interface as a function of axial height Z for soft and stiff fibers. Three values of embedded length are studied for: 0.1 times the matrix height, 0.4 times the matrix height and 0.8 times the matrix height.

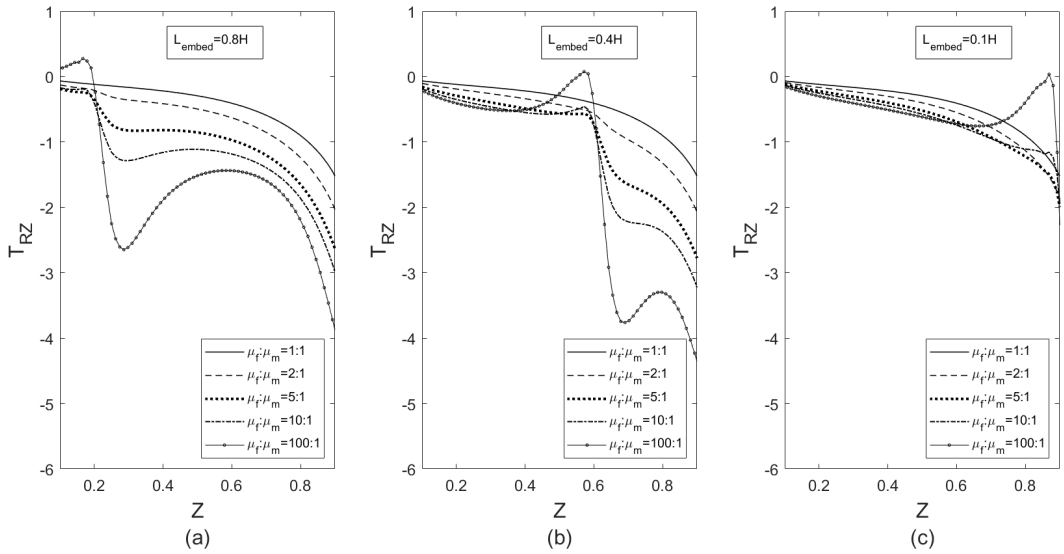

Figure 3.2: Interfacial Shear stress for different embedded lengths: a) $0.2H$, b) $0.4H$, c) $0.1H$ for partially embedded fiber-matrix system fixed at the circumference

In figure 3.1a, where a larger length of the fiber is embedded into the matrix, the stiffer fiber shows a larger region of uniform distribution of shear stress than that of the cases where the embedded length of the fiber is shorter, (figure 3.1b and 3.1c). This is because, as the fiber embedded length increases for a stiffer fiber, a larger region of the matrix deforms, thereby generating a uniform shear stress in the surrounding matrix along the embedded length. However, for soft fibers,

the interfacial shear stress distribution is not uniform and does not depend on the embedded length of the fiber. Figure 3.3 and figure 3.4 show the shear stress contour plot with embedded lengths varying from $0.1H$ to $0.9H$ for a soft and a stiff fiber respectively.

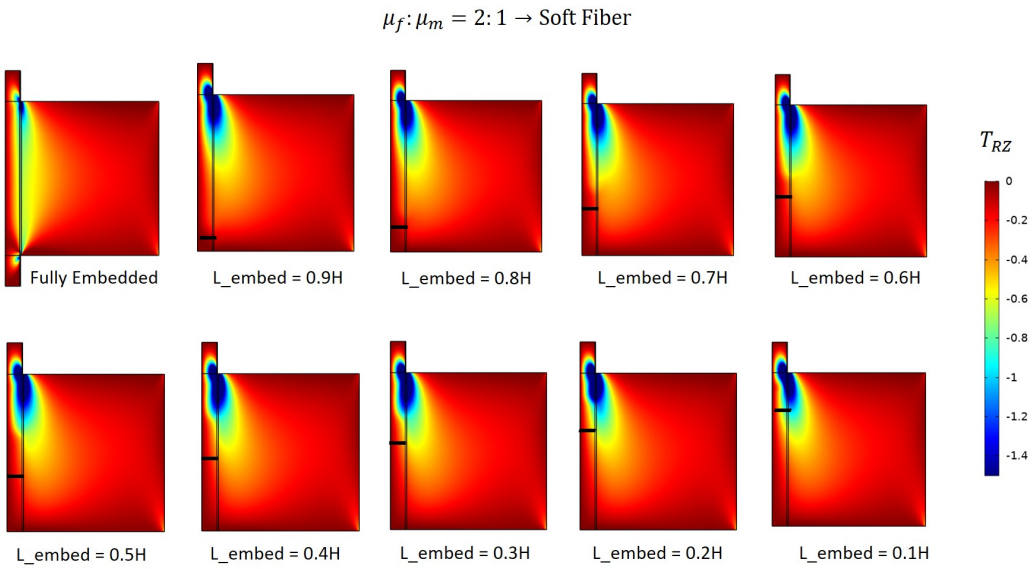

Figure 3.3: Shear stress distribution for partially embedded fiber-matrix system fixed at the circumference for soft fiber $(\mu_f : \mu_m) = 2:1$

From figure 3.3 it can be observed that the shear stress distribution is independent of the embedded length of the fiber. Additionally, for a soft fiber, the deformation is localized at the top portion of the fiber and there is negligible deformation in the matrix. Therefore, the shear stress is lower in magnitude in the case of a soft fiber. Whereas, figure 3.4 shows that for a stiff fiber, the embedded length of the fiber has a significant effect on the shear stress distribution. As the embedded length increases, the shear stress increases and the distribution is much uniform in the matrix region along the embedded length.

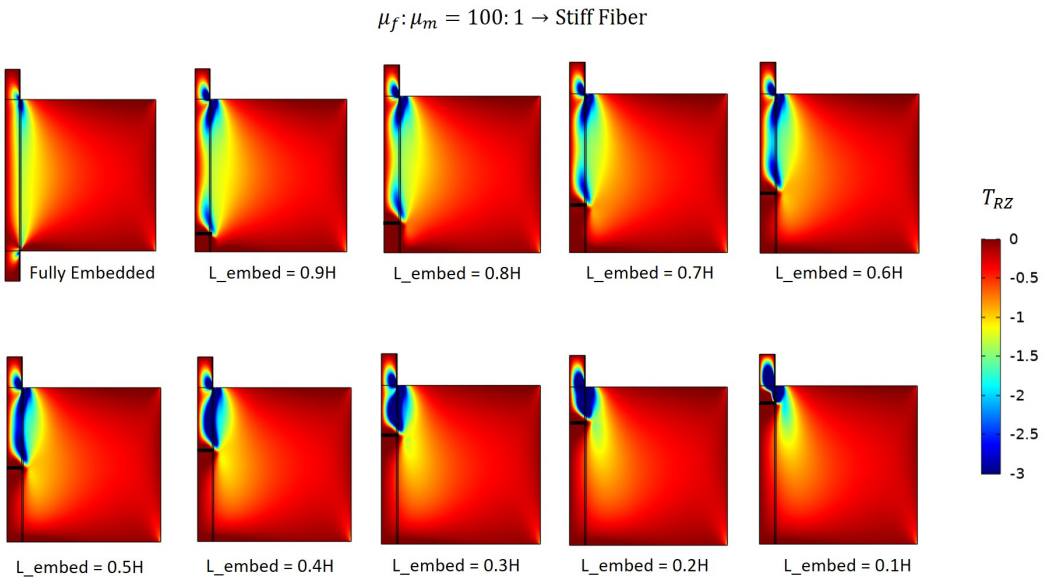

Figure 3.4: Shear stress distribution for partially embedded fiber-matrix system fixed at the circumference for a stiff fiber $(\mu_f : \mu_m) = 100 : 1$

3.3 Pullout Force

In this section, the dependence of the force required to pull the fiber on the material parameters of the fiber and the matrix is examined. Figure 3.5 shows the variation of the pullout force with displacement for different geometrical and material parameters. It is observed that the pullout force increases with an increase in the fiber shear modulus. When $\mu_f : \mu_m$ is close to 1, most of the deformation occurs in the portion of the fiber, extending beyond the matrix, resulting in small to negligible deformation in the matrix. As the shear modulus of the fiber increases, an increasingly larger region of the matrix deforms causing an increase in the pullout force. This can be observed from figure 3.6 where the deformation in the matrix increases with increasing μ of the fiber.

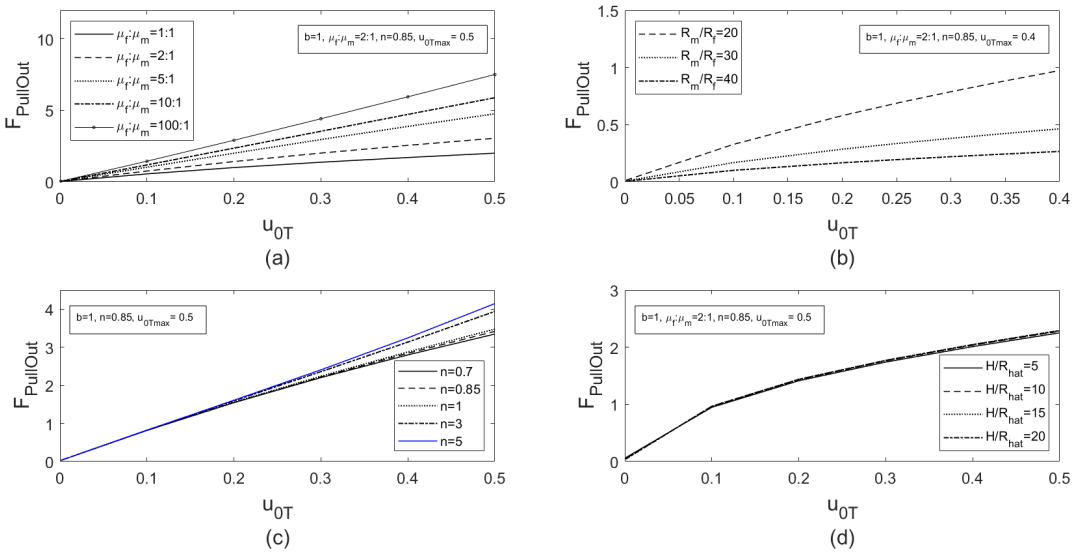

Figure 3.5: Pull out force vs displacement of the top surface of the fiber (u_{0T}) for a) varying shear modulus ratio $(\mu_f : \mu_m)$, b) radius ratio R_m/R_f, c) power-law constant n, d) non-dimensional number $H/\hat{R}$ respectively for partially embedded fiber with fixed outer surface. (The force is calculated at the top surface of the fiber where (u_{0T}) is applied)

The pullout force decreases with a decrease in the radius of the fiber. In the case of a thin fiber, most of the deformation occurs in the part of the fiber, extending beyond the matrix. With an increase in the fiber radius, a larger region of the matrix deforms, resulting in an increase in the pullout force. The material parameter n and the geometric parameter H/R seem to have little effect on the pullout force within the range of displacements (u_{0T}) simulated here.

The effect of the above parameters on the axial displacement of the fiber and the matrix is shown in figure 3.6.

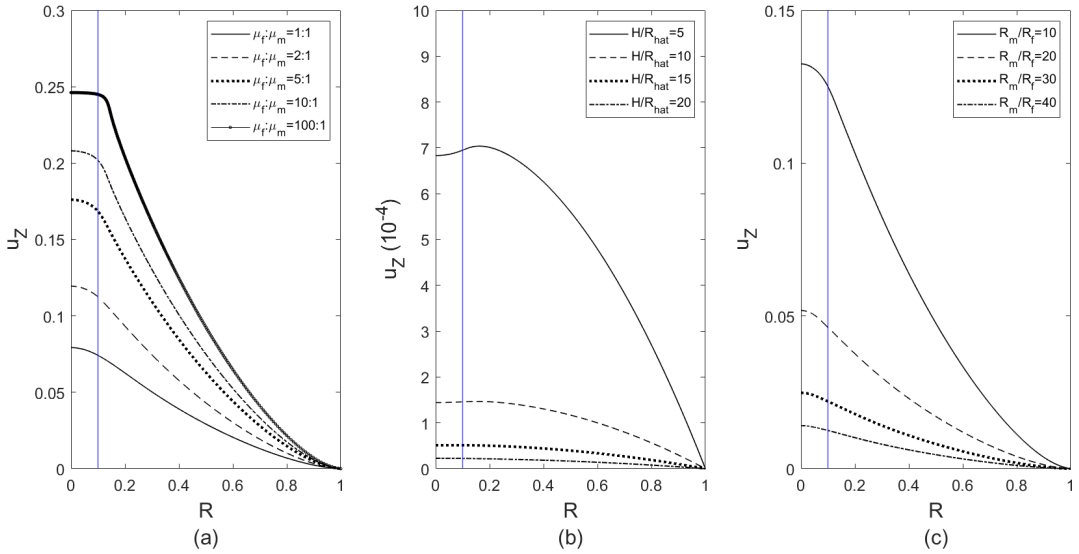

Figure 3.6: Axial displacement as a function of radial distance for a) varying shear modulus ratio $(\mu_f : \mu_m)$, b) non-dimensional number $(H/\hat{R})$ & c) radius ratio (R_m/R_f) respectively for partially embedded fiber with fixed outer surface. ($n_f = 1$, $n_m = 0.6$, $b_f = b_m = 1$, $u_{0T} = 0.25$) (The values are taken at $z = 0.5$ along a radial line extending from $r = 0$ to $r = R_0$. The blue line shows the fiber-matrix interface)

From figure 3.6, it is observed that the displacement is highest at the fiber end and gradually reduces to zero at the outer surface boundary. It increases with an increase in the fiber stiffness due to the deformation in a larger region of the matrix. Similarly, as the fiber radius decreases, a reduction in the axial displacement can be observed. This is due to the localization of the deformation in the fiber and small to negligible deformation occurring in the matrix. Further, as the geometric parameter $H/\hat{R}$ increases, the model behaves like an infinite cylinder and the deformation is localized only in the portion of the fiber extending beyond the matrix. This explains the reduction in the displacement with an increase in $H/\hat{R}$. Moreover, it reduces significantly on increasing the parameter from a value of 5 to 10, after which the reduction is less significant.

Having discussed the force and the displacement, the strain is examined, in terms of the norm of the strain tensor. The norm of the strain tensor is plotted as a function of radial distance at different heights, along the axial direction $(at\ z = 0.2, z = 0.5, z = 0.6, z = 0.8, z = 0.9)$ for two different ratios of shear modulus $(\mu_f : \mu_m) = 2 : 1$ and $(\mu_f : \mu_m) = 10 : 1$, as shown in figure 3.7

for the boundary value problems.

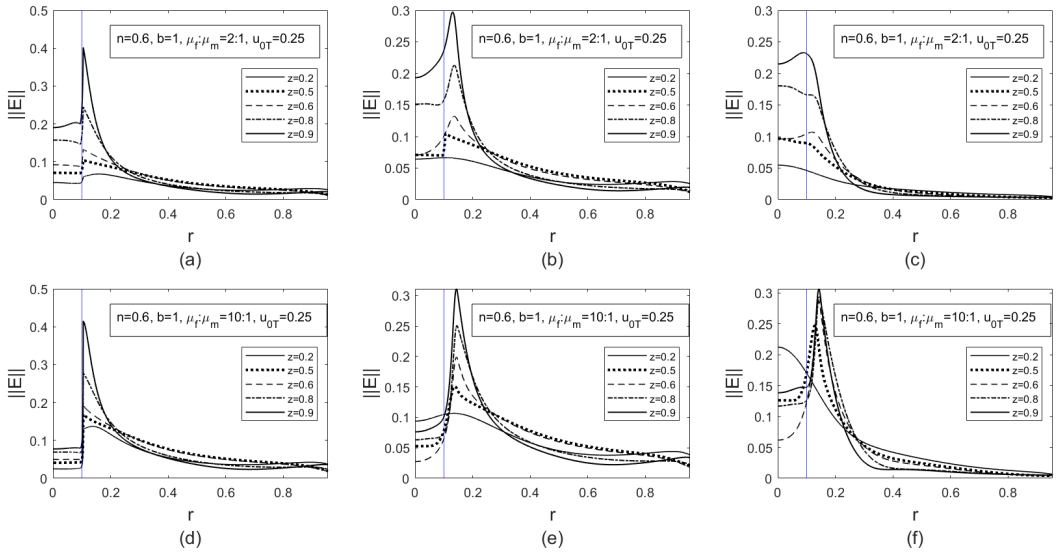

Figure 3.7: a) & b) Norm of strain tensor as a function of radial distance for fully and partially embedded fiber respectively with fixed outer surface, c) partially embedded fiber respectively with fixed bottom with $\mu_f : \mu_m = 2 : 1$. e) & f) Norm of strain tensor as a function of radial distance for fully and partially embedded fiber respectively with fixed outer surface g) partially embedded fiber respectively with fixed bottom for $\mu_f : \mu_m = 10 : 1$, at different axial distance $(z = 0.2, z = 0.5, z = 0.6, z = 0.8, z = 0.9)$. (Blue vertical line indicates the fiber-matrix interface)

It can be observed from 3.7a, 3.7b and 3.7c that the norm of the strain tensor increases as one approaches the top surface of the matrix for the fully and the partially embedded fiber problems. This is due to the similar stiffness ratio of the fiber and the matrix ($\mu_f : \mu_m = 2 : 1$) where most of the deformation occurs in the region of the fiber extending beyond the matrix and the region of the matrix, close to the top surface of the matrix (i.e $z = 0.9$). As the fiber becomes stiffer ($\mu_f : \mu_m = 10 : 1$), a larger portion of the matrix deforms, leading to a higher value of the strain in the matrix along the entire interface. Therefore, a significantly higher magnitude is observed for the norm of strain tensor at $z = 0.5$ in this case (see figure 3.7d, 3.7e and 3.7f).

3.4 Parametric Study

In this section, the deformations and the stresses related to the fiber pullout problem, and their dependencies on various model parameters are studied. The following material parameters which appear to have significant effects on the force required for the fiber pullout are considered here. The ratio of the shear modulus of the fiber to the matrix $(\mu_f : \mu_m)$ is varied from 1 to 10. The radius ratio, defined as the ratio of outer radius of matrix to that of fiber (R_m/R_f), is varied from 10 to 40. Further, the non-dimensional parameter $(H/\hat{R})$ is varied from 5 to 20. The values of stress in the figures are taken at $z = 0.5$ along a radial line extending from $r = 0$ to $r = 1$.

3.4.1 Varying Shear Modulus

Figure 3.8 shows the shear stress distribution as a function of the radial distance and figure 3.9 shows a contour plot of the shear stress distribution with different shear modulus ratios when $u_{0T} = 0.25$.

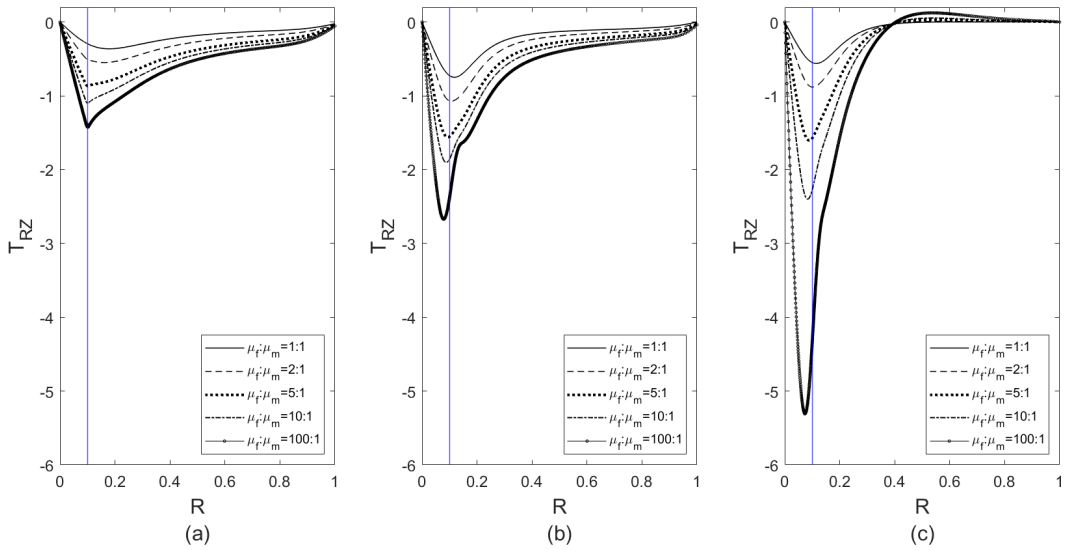

Figure 3.8: Shear stress distribution as a function of radial distance for a) fully embedded fiber with fixed outer surface, b) partially embedded fiber with fixed outer surface, c) partially embedded fiber with fixed bottom respectively with varying shear modulus ratio. ($n_f = 1$, $n_m = 0.6$, $b_f = b_m = 1$, $R_m/R_f = 10$, $\hat{R}/H = 2$, $u_{0T} = 0.25$. The values are taken at $z = 0.5$ along a radial line extending from $r = 0$ to $r = R_m$. The blue line shows the fiber-matrix interface)

The shear stress is zero at the fiber inner radius. As one approaches towards the fiber-matrix interface, the shear stress reaches a peak value, after which it gradually decreases with increasing r. Unlike the case of very stiff fibers embedded in a soft matrix, when the shear modulus of the fiber is close to that of the matrix, the peak shear stress does not occur at the interface. It occurs within the matrix region for both the fully and the partially embedded fiber problems.

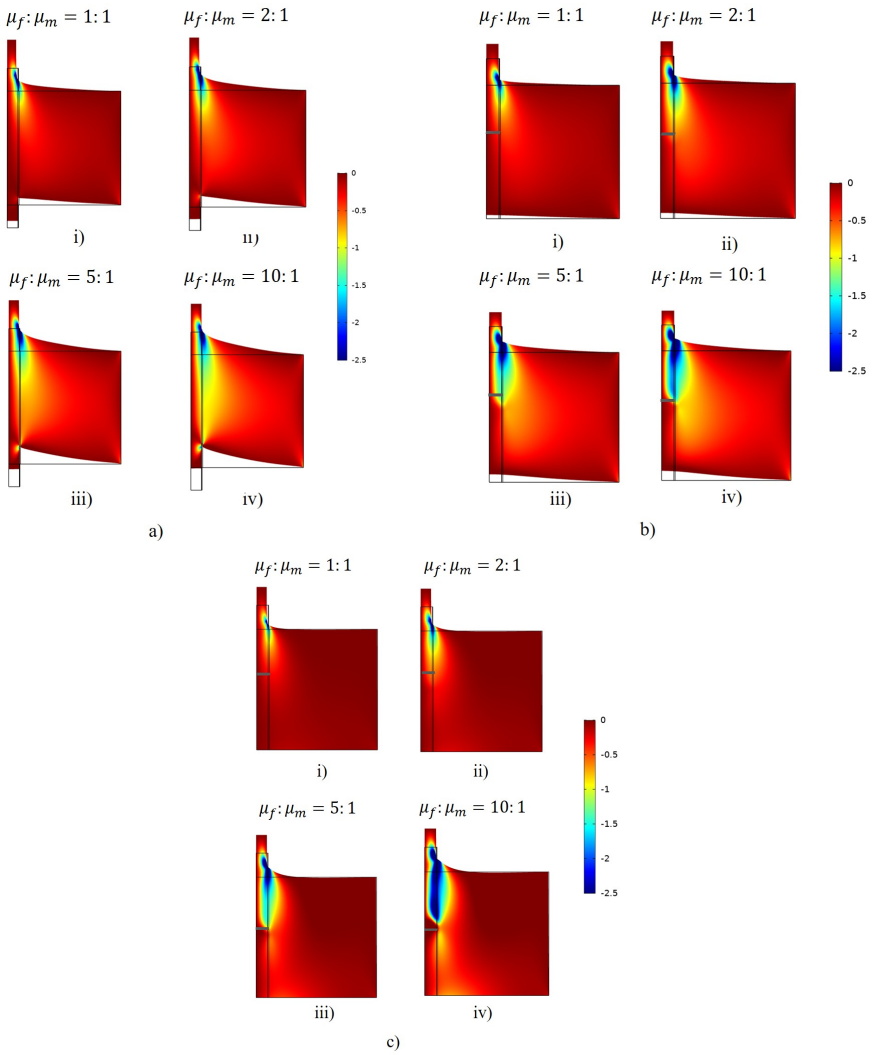

Figure 3.9: a) Shear Stress with Varying shear modulus ratio for fully embedded fiber with fixed outer surface. b) Shear Stress with Varying shear modulus ratio for partially embedded fiber with fixed outer surface. c) Shear Stress with Varying shear modulus ratio for partially embedded fiber with fixed bottom. ($n_f = 1$, $n_m = 0.6$, $b_f = b_m = 1$, $R_m/R_f = 10$, $\hat{R}/H = 2$, $u_{0T} = 0.25$)

As the fiber's shear modulus increases, the peak shifts towards the interface as can be seen from figures 3.8a and 3.9a & b. Also, with an increase in the shear modulus of the fiber, deformation of the matrix increases, causing an increase in the shear stress at the fiber-matrix interface. It can be observed from figure 3.9, that a larger region of the matrix experiences higher shear stress when the ratio of the fiber shear modulus to the matrix shear modulus increases.

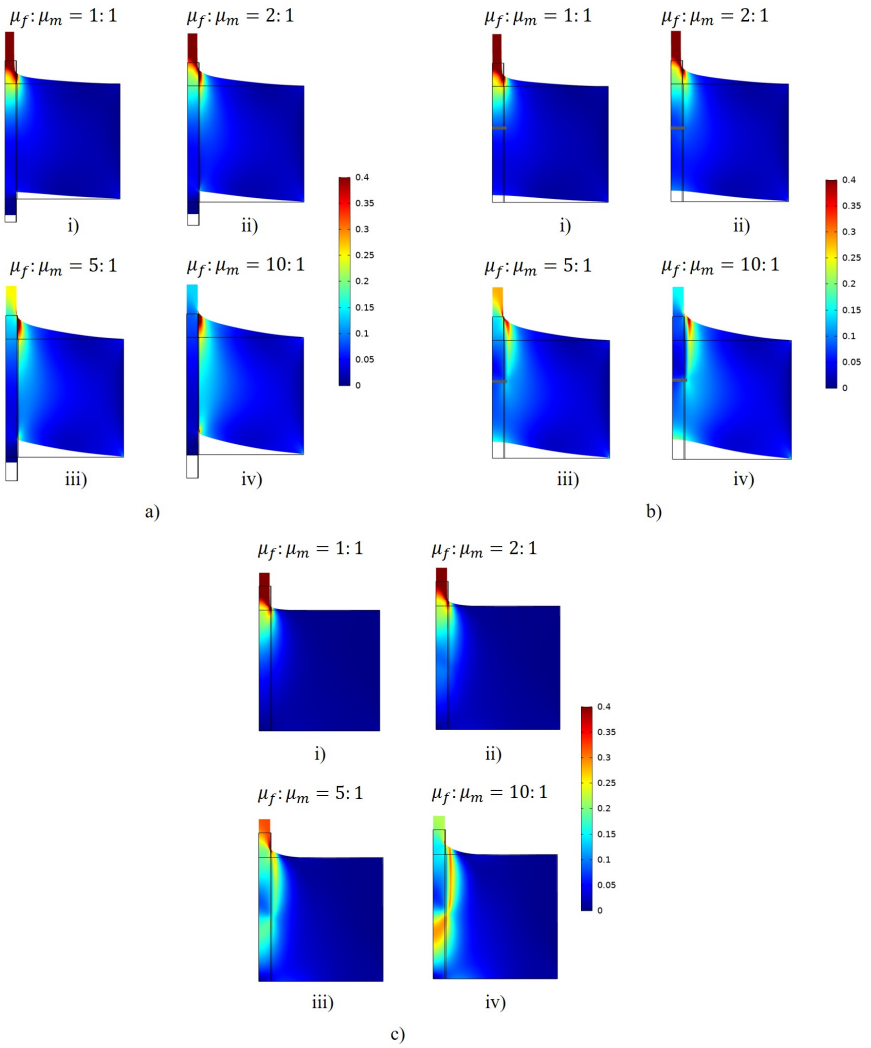

Figure 3.10: a) Norm of strain tensor with Varying shear modulus ratio for fully embedded fiber with fixed outer surface, b) partially embedded fiber with fixed outer surface, c) partially embedded fiber with fixed bottom ($n_f = 1$, $n_m = 0.6$, $b_f = b_m = 1$, $R_m/R_f = 10$, $\hat{R}/H = 2$, $u_{0T} = 0.25$). (where the norm of strain tensor is given by: $||\mathbf{E}|| = (tr(\mathbf{E}^T\mathbf{E}))^{1/2}$).

Figure 3.10 shows the norm of shear strain, $||E||$. As the fiber stiffness increases, a larger portion of the matrix deforms, leading to a higher strain in the matrix along the entire interface, as can be seen in figure 3.10a, iii & iv, 3.10b, iii & iv and 3.10c, iii & iv.

In the next sections, the influence of the geometric parameters will be studied on the pullout problem.

3.4.2 Varying Radius Ratio

Here, the impact of varying radius ratios on the deformation and the shear stress distribution is considered. The radius ratio is defined as the ratio of the outer radius of the matrix to that of the fiber (R_m/R_f). Figure 3.11 shows the stress distribution as a function of the radial distance with different R_m/R_f.

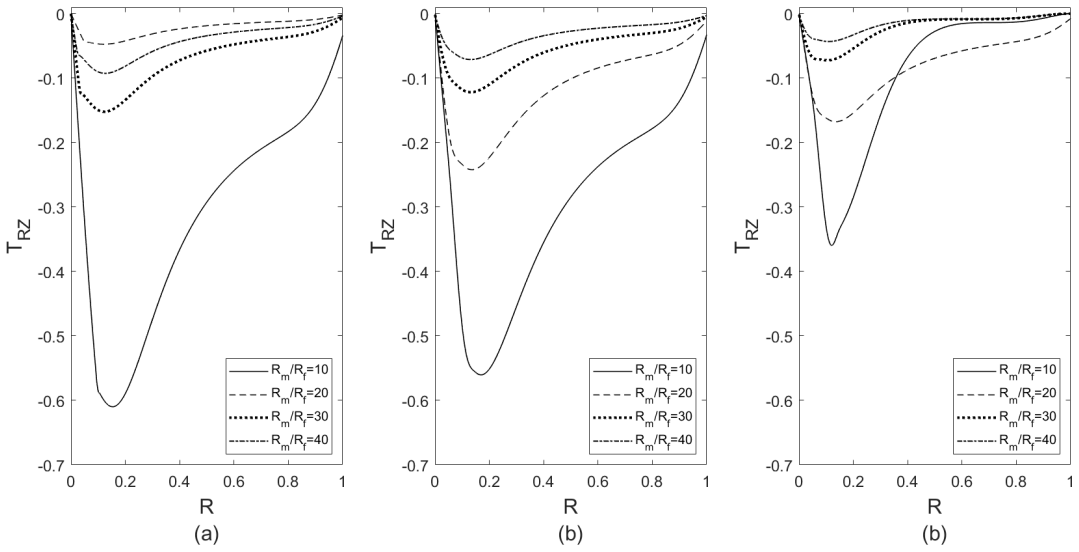

Figure 3.11: Shear stress distribution as a function of radial distance for a) fully embedded fiber with fixed outer surface, b) partially embedded fiber with fixed outer surface, c) partially embedded fiber with fixed bottom respectively with radius ratio. ($n_f = 1$, $n_m = 0.6$, $b_f = b_m = 1$, $\mu_f : \mu_m = 2 : 1$, $\hat{R}/H = 2$, $u_{0T} = 0.25$. The values are taken at $z = 0.5$ along a radial line extending from $r = 0$ to $r = R_m$)

It is observed that the shear stress decreases with a decrease in the radius of the fiber. In the

case of a thin fiber, most of the deformation occurs in the fiber portion extended beyond the matrix. With an increase in the fiber radius, a larger region of the matrix deforms resulting in an increase in the shear stress as is seen in figure 3.11.

3.4.3 Varying Geometric Parameter $R/\hat{H}$

In this section, the dependence of the solutions on the geometric parameter $H/\hat{R}$ is considered.

Figure 3.12 shows the variation of the stress distribution as a function of radial distance with different values of the geometric parameter $H/\hat{R}$ of $(5, 10, 15, 20)$.

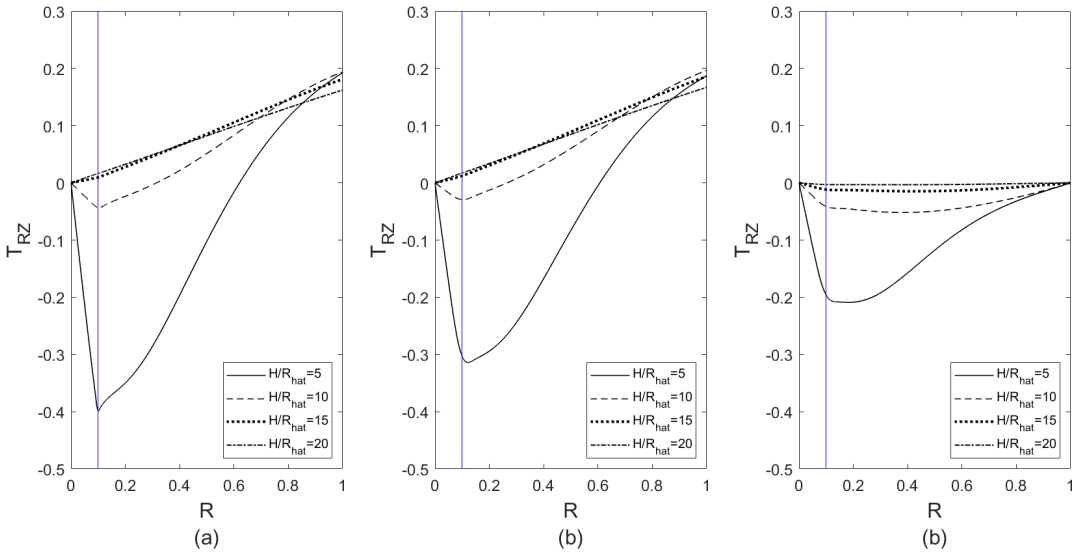

Figure 3.12: Shear stress distribution as a function of radial distance for a) fully embedded fiber with fixed outer surface, b) partially embedded fiber with fixed outer surface, c) partially embedded fiber with fixed bottom respectively with non-dimensional parameter $H/\hat{R}$. ($n_f = 1$, $n_m = 0.6$, $b_f = b_m = 1$, $\mu_f : \mu_m = 2 : 1$, $R_m/R_f = 10$, $u_{0T} = 0.25$. The values are taken at $z = 0.9$ along a radial line extending from $r = 0$ to $r = R_m$). The blue line shows the fiber-matrix interface.

Here, as $H/\hat{R}$ increases, the model behaves like an infinite cylinder and the deformation is localized in the extended portion of the fiber beyond the matrix. As a result, the peak shear stress can be observed near the top end of the matrix, hence the axial location $Z = 0.9$ is chosen to plot the shear stress distribution with varying $H/\hat{R}$. The remaining region of the fiber-matrix system

shows negligible deformation in case of a higher $H/\hat{R}$, thereby reducing the peak shear stress, as is seen from figure 3.12. Further, for figure 3.12c, since the bottom of the matrix is fixed, the shear stress behavior is different than that of figure 3.12a & figure 3.12b. The shear stress reduces to zero at the traction-free outer surface for the third boundary value problem, whereas, the shear stress has considerable magnitude near the matrix outer circumference for the first two boundary value problems. Additionally, on stiffening the fiber, an increasingly larger region of the matrix deforms, increasing the absolute peak shear stress. (The depth of the peaks in the above figure3.12 is expected to shift down axially along Z).

Finally, the influence of material parameters n and b is also examined. They seem to have a negligible effect on the shear stress distribution as shown in figure 3.13

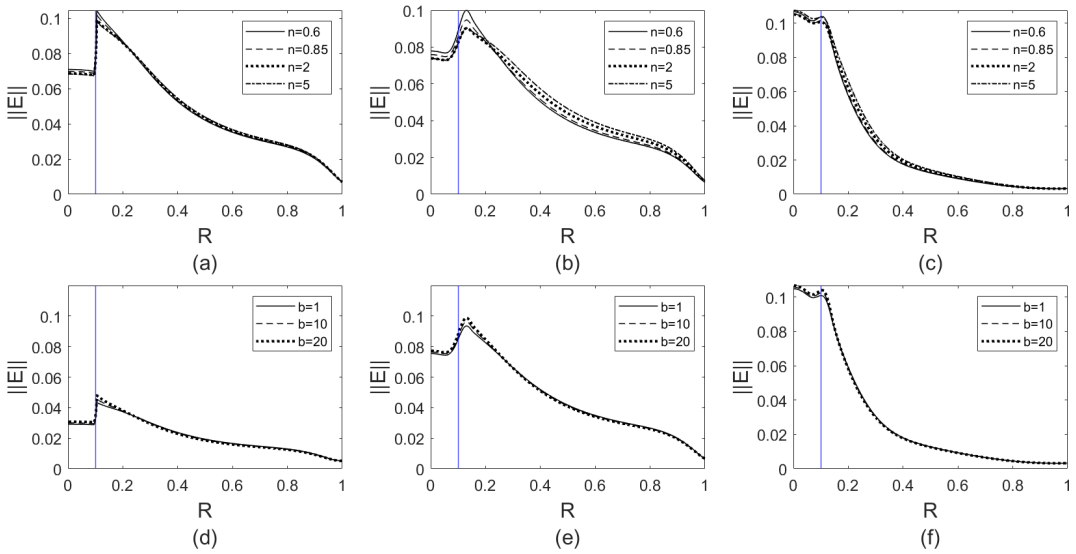

Figure 3.13: Shear stress distribution as a function of radial distance for a) fully embedded fiber with fixed outer surface, b) partially embedded fiber with fixed outer surface, c) partially embedded fiber with fixed bottom respectively with varying n, d) fully embedded fiber with fixed outer surface, e) partially embedded fiber with fixed outer surface, f) partially embedded fiber with fixed bottom respectively with varying b. ($\mu_f : \mu_m = 2 : 1$, $R_m/R_f = 10$, $\hat{R}/H = 2$, $u_{0T} = 0.25$. The values are taken at $z = 0.5$ along a radial line extending from $r = 0$ to $r = R_m$). The blue line shows the fiber-matrix interface.

Figure 3.13 shows that the shear strain forms a boundary layer at the interface where there is a

smooth transition of the material properties from the fiber to the matrix.

3.4.4 Effect of Compressibility

In most of the studies on polymers, a nearly incompressible behavior is assumed and a high bulk modulus to shear modulus ratio is used. In all the previous results in the work, a K/μ of 100 is used to represent the nearly incompressible behavior. In the following, a brief comment is made on the influence of K/μ on the stress distributions in the fiber and the matrix during a fiber pullout.

In this sub-section, a discussion is made about the influence of bulk modulus in the solutions. In this work, the K_{factor} is defined as the ratio of K to μ, which is varied from 10 to 1000, and the stress distribution is observed as a function of radial distance.

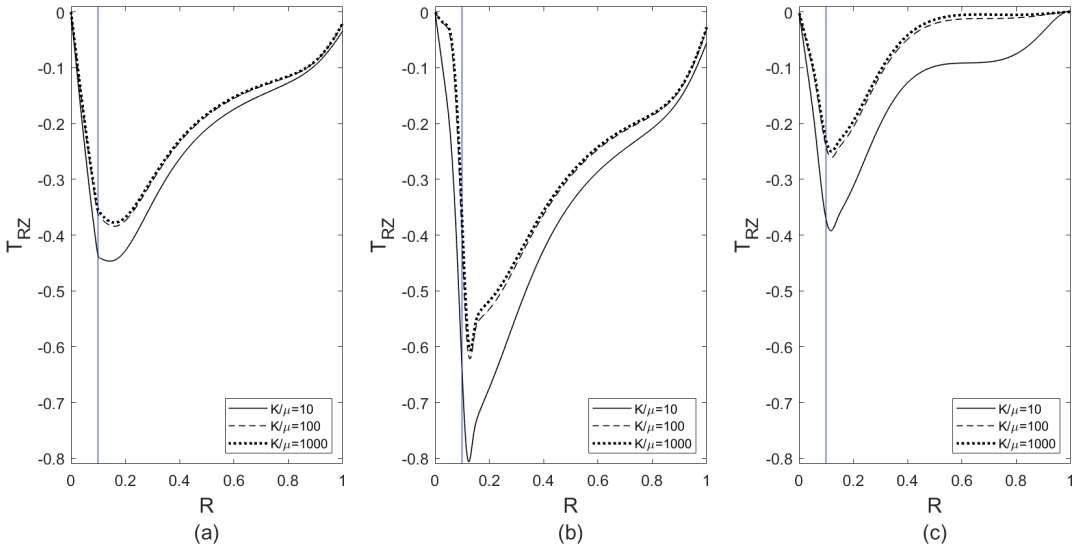

Figure 3.14: Shear stress distribution as a function of radial distance for a) fully embedded fiber with fixed outer surface, b) partially embedded fiber with fixed outer surface, c) partially embedded fiber with fixed bottom respectively with varying K_{factor}. ($n_f = 1$, $n_m = 0.6$, $b_f = b_m = 1$, $\mu_f : \mu_m = 2 : 1$, $R_m/R_f = 10$, $H/\hat{R} = 1$, $u_{0T} = 0.25$. The values are taken at $z = 0.5$ along a radial line extending from $r = 0$ to $r = R_m$). The blue line shows the fiber-matrix interface.

From figure 3.14, it is observed that, as the K_{factor} increases, the shear stress reduces. The fiber and the matrix are less compressible, in turn, reducing the stresses in the system. For a

compressible fiber-matrix system, i.e., $K_{factor} = 10$, the fiber and the matrix deform largely, increasing the shear stress.

3.5 Comparison of the Boundary Value Problems

In this section, the overall behavior of the boundary value problems is analyzed. A brief description is made on the similarities and the differences in the deformation and the stress distributions for the fully and the partially embedded fiber-matrix geometries and the different boundary conditions.

Figure 3.15 shows the stress distribution and the deformation for the entire fiber-matrix domain. In this section, the simulations are performed with parameter values as $n_{fiber} = 1,\ b_{fiber} = 1,\ n_{matrix} = 0.6,\ b_{matrix} = 1,\ \mu_{fiber} : \mu_{matrix} = 2 : 1,\ \hat{R}/H = 2,\ R_m/R_f = 10,\ u_{0T} = 0.25$ for first two problems and $u_{0T} = 0.15$ for the third problem. For all the conditions, the top extended portion of the fiber, where the displacement (u_{0T}) is applied, deforms largely. The deformation then gradually reduces as one moves away from the top surface of the matrix. The problems where the outer surface is fixed, the matrix portion adjacent to the outer surface shows negligible deformation, as can be seen from figures 3.15-a-i and 3.15-b-i. For the third problem, where the bottom of the matrix is fixed, a major region of the matrix shows negligible deformation (figure 3.15-c-i).

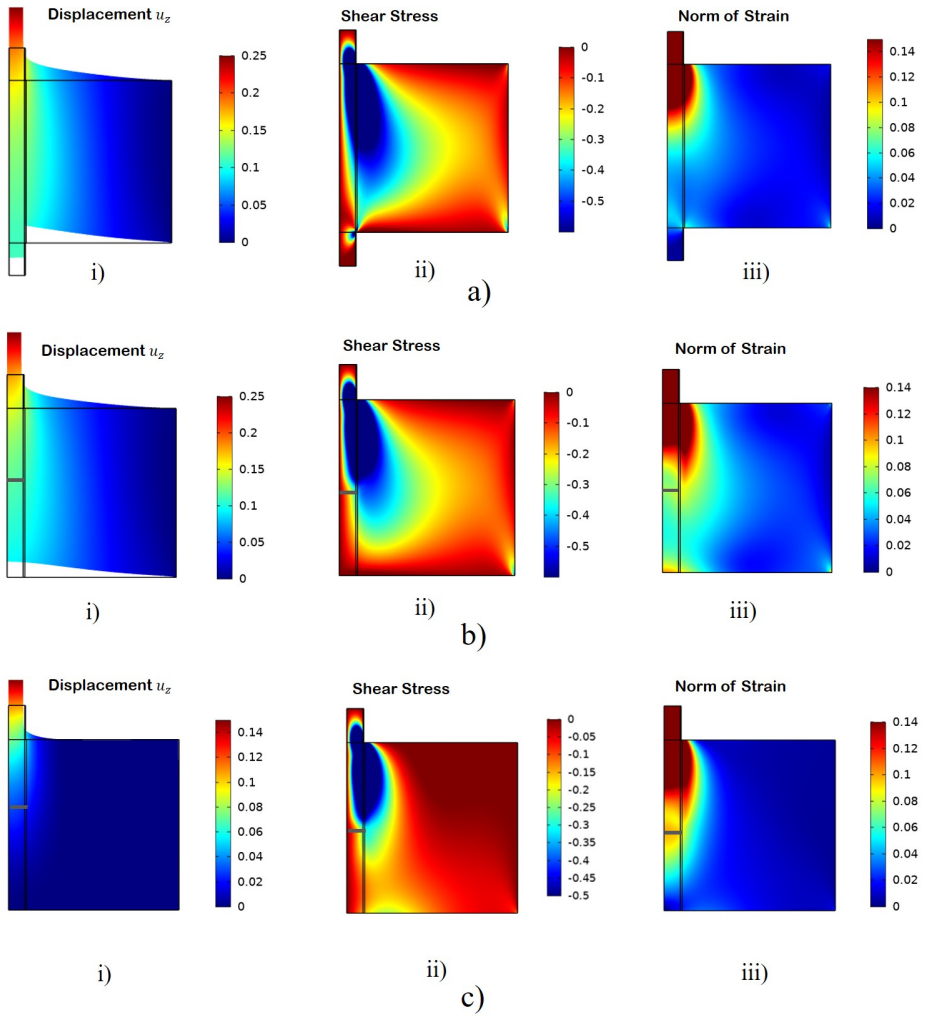

Figure 3.15: Deformation & Stress plots (2D). a) Fully Embedded Fiber with fixed outer surface, b) Partially Embedded Fiber with fixed outer surface, c) Partially Embedded Fiber with fixed bottom. ($n_{fiber} = 1$, $b_{fiber} = 1$, $n_{matrix} = 0.6$, $b_{matrix} = 1$, $\mu_f : \mu_m = 2 : 1$, $\hat{R}/H = 2$, $R_m/R_f = 10$, $u_{0T} = 0.25$.)

The pullout displacement u_{0T} causes a shearing effect generating high shear stress at the interface. In figure 3.15-a-ii, the matrix deforms more in the case of a fully embedded fiber compared to the partially embedded fiber. Hence the shear stress is significant in a larger region near the interface than that in figure 3.15-b-ii when the fiber is partially embedded. In addition, the matrix shows negligible deformation close to the outer surface in case of a fully embedded fiber, and at the outer and the bottom surfaces in case of a partially embedded fiber (figure 3.15-a-ii, figure

3.15-b-ii). The shear stress thus reduces to nearly zero values in the matrix region away from the interface. However, when the matrix is held fixed at the bottom (figure 3.15-c-ii), the magnitude of the shear stress is considerable near the bottom of the matrix with negligible shear stress near the traction-free outer surface.

Finally, a comparison is made on the strains for the boundary value problems. Figure 3.15-a-iii, 3.15-b-iii and 3.15-c-iii show the norm of the shear strain in the model. For the shear modulus ratio $\mu_f/\mu_m = 2 : 1$, both the fiber and the matrix deform. However, most of the deformation is localized in the fiber as shown by the norm of the strain being high at the extended portion of the fiber and a small region in the matrix along the interface near the top surface of the matrix for both the problems. The deformation is negligible in the matrix region away from the interface and the strain is nearly zero at the fixed boundaries (matrix outer surface for first two problems; figure 3.15-a-iii & figure 3.15-b-iii and matrix bottom for the third problem; figure 3.15-c-iii).

4. SUMMARY AND CONCLUSION

4.1 Conclusion

In this thesis, the deformation and the stress experienced by a cylindrical fiber-matrix system are studied, where the fiber-matrix system is subjected to an axial pull-out displacement during a pullout phenomenon. The three boundary value problems are considered: a fully embedded fiber with the matrix being held at the matrix circumference and a partially embedded fiber held at the bottom of the geometry. The effect of the material and the geometric parameters on the boundary value problems is analyzed. Additionally, the behavior of interface shear stress and the force required to achieve a particular range of pull-out displacements are studied. From this study, certain conclusions can be drawn.

Based on the discussions from the previous section, certain conclusions can be drawn for this study. The interfacial shear stress was thoroughly studied in past literature where fibers that were stiffer as compared to matrix, were considered. However, on studying the interfacial shear stress for both soft and stiff fibers in this work, it can be found that, for a soft fiber, the interfacial shear stress is not uniform. Further, as the fiber becomes stiffer, the interfacial shear stress increases. On performing the stress analysis, it is concluded that for a soft fiber, most of the deformation is localized in the fiber portion extending beyond the matrix, however, for a stiff fiber, an increasingly larger region of the matrix deforms. As a result, the pullout force required for the given pullout displacement and the interfacial shear stress is higher for a stiff fiber than that of a soft fiber. In the pullout tests performed in the past, the force required to pullout the fiber was measured. The conclusion obtained about the pullout force in this work will aid in similar future pullout tests. Further, a stiff fiber-matrix system has higher strain along the interface, whereas, a soft fiber-matrix system has relatively higher strain near the portion of fiber & matrix where the pullout displacement is applied.

A significant conclusion can be made on the shear stress distribution. For a soft fiber, the peak

shear stress occurs within the matrix region as compared to that of a stiff fiber, where the peak shear stress occurs at the fiber-matrix interface.

On studying the geometric parameters, it is concluded that, for a thin fiber, a larger region of the matrix deforms as compared to a thicker fiber which leads to higher shear stress. On increasing the $H/\hat{R}$, the deformation is localized in the extended portion of the fiber, thereby reducing the shear stress. Further, it is noted that, as the system becomes more compressible, the shear stress at the interface reduces.

For the problem with the fixed outer surface of the matrix, a larger region of the interface shows a significant displacement, however, in the case where the bottom of the system is fixed, there is negligible deformation in the matrix. For a fully embedded fiber, a larger region of the system has a stiffer component. Hence, the shear stress is significant in a larger region of the matrix adjacent to the interface. Whereas, for a partially embedded fiber, the shear stress is negligible in most of the regions in the matrix. Further, for the two different boundaries, the shear stress distribution changes according to the boundary which is held fixed. Due to similar reasons, the partially embedded fiber exhibits higher strain in the system interface than the fully embedded fiber. Additionally, deformation in the matrix is higher when it is held from the outer surface, as compared to the case when it is fixed in the bottom.

4.2 Future Studies

In the future, this study can be extended to an analytical formulation of the debond forces arising due to the axial pullout for the same fiber-matrix system. The interfacial shear strength is essentially the slope of the debond-force and debond-length curve. The stress and deformation obtained here can be used to have a rough estimation of the slope in conjunction with pullout tests in the future. Further, fiber pullout experiments can be conducted to represent and validate the analytical studies conducted in this work. For pullout experiments, a hard plastic as a fiber, embedded in a silicone matrix can be considered. The stiffness of the plastic can be varied to conform to the parameters of the experiments being conducted.

REFERENCES

[1] A. Gent and O. Yeoh, "Failure loads for model adhesive joints subjected to tension, compression or torsion," *Journal of Materials Science*, vol. 17, no. 6, pp. 1713–1722, 1982.

[2] C.-H. Hsueh, "Interfacial debonding and fiber pull-out stresses of fiber-reinforced composites vii: improved analyses for bonded interfaces," *Materials Science and Engineering: A*, vol. 154, no. 2, pp. 125–132, 1992.

[3] C. Yue and W. Cheung, "Interfacial properties of fibrous composites," *Journal of materials science*, vol. 27, no. 12, pp. 3181–3191, 1992.

[4] T. Abu-Lebdeh, S. Hamoush, W. Heard, and B. Zornig, "Effect of matrix strength on pullout behavior of steel fiber reinforced very-high strength concrete composites," *Construction and Building Materials*, vol. 25, no. 1, pp. 39–46, 2011.

[5] H. Stang and S. Shah, "Failure of fibre-reinforced composites by pull-out fracture," *Journal of materials science*, vol. 21, no. 3, pp. 953–957, 1986.

[6] C.-H. Hsueh, "Interfacial debonding and fiber pull-out stresses of fiber-reinforced composites," *Materials Science and Engineering: A*, vol. 123, no. 1, pp. 1–11, 1990.

[7] P. Di Maida, E. Radi, C. Sciancalepore, and F. Bondioli, "Pullout behavior of polypropylene macro-synthetic fibers treated with nano-silica," *Construction and Building Materials*, vol. 82, pp. 39–44, 2015.

[8] J. L. Holloway, A. M. Lowman, M. R. VanLandingham, and G. R. Palmese, "Chemical grafting for improved interfacial shear strength in uhmwpe/pva-hydrogel fiber-based composites used as soft fibrous tissue replacements," *Composites science and technology*, vol. 85, pp. 118–125, 2013.

[9] A. Gent, G. Fielding-Russell, D. Livingston, and D. Nicholson, "Failure of cord-rubber composites by pull-out or transverse fracture," *Journal of Materials Science*, vol. 16, no. 4,

pp. 949–956, 1981.

[10] S. Zhang, S. Li, M. Jia, Y. Hao, and R. Yang, "Fatigue properties of a multifunctional titanium alloy exhibiting nonlinear elastic deformation behavior," *Scripta Materialia*, vol. 60, no. 8, pp. 733–736, 2009. cited By 42.

[11] W. R. Illeperuma, J.-Y. Sun, Z. Suo, and J. J. Vlassak, "Fiber-reinforced tough hydrogels," *Extreme Mechanics Letters*, vol. 1, pp. 90–96, 2014.

[12] H.-H. Zhu, C.-C. Zhang, C.-S. Tang, B. Shi, and B.-J. Wang, "Modeling the pullout behavior of short fiber in reinforced soil," *Geotextiles and Geomembranes*, vol. 42, no. 4, pp. 329–338, 2014.

[13] S. Ziraki, S. M. Zebarjad, and M. J. Hadianfard, "A study on the tensile properties of silicone rubber/polypropylene fibers/silica hybrid nanocomposites," *Journal of the Mechanical Behavior of Biomedical Materials*, vol. 57, pp. 289–296, 2016.

[14] C.-H. Hsueh, "Interfacial debonding and fiber pull-out stresses of fiber-reinforced composites iii: With residual radial and axial stresses," *Materials Science And Engineering: A*, vol. 145, no. 2, pp. 135–142, 1991.

[15] C. Marotzke, "The elastic stress field arising in the single-fiber pull-out test," *Composites science and technology*, vol. 50, no. 3, pp. 393–405, 1994.

[16] Y. Zhao, Y. Xing, Z. Lei, and F. Lang, "Interfacial stress transfer behavior in a specially-shaped fiber/matrix pullout test," *Acta Mechanica Sinica*, vol. 26, no. 1, pp. 113–119, 2010.

[17] S.-Y. Fu, C.-Y. Yue, X. Hu, and Y.-W. Mai, "Analyses of the micromechanics of stress transfer in single-and multi-fiber pull-out tests," *Composites science and technology*, vol. 60, no. 4, pp. 569–579, 2000.

[18] Q.-S. Yang, Q.-H. Qin, and X.-R. Peng, "Size effects in the fiber pullout test," *Composite structures*, vol. 61, no. 3, pp. 193–198, 2003.

[19] M. Frikha, H. Nouri, S. Guessasma, F. Roger, and C. Bradai, "Interfacial behaviour from pull-out tests of steel and aluminium fibres in unsaturated polyester matrix," *Journal of Materials Science*, vol. 52, no. 24, pp. 13829–13840, 2017.

[20] L. S. Penn and S. M. Lee, "Interpretation of experimental results in the single pull-out filament test," *Journal of Composites, Technology and Research*, vol. 11, no. 1, pp. 23–30, 1989.

[21] R. J. Kerans and T. A. Parthasarathy, "Theoretical analysis of the fiber pullout and pushout tests," *Journal of the American Ceramic Society*, vol. 74, no. 7, pp. 1585–1596, 1991.

[22] O. Kononova, V. Lusis, A. Galushchak, A. Krasnikovs, and A. Macanovskis, "910. numerical modeling of fiber pull-out micromechanics in concrete matrix composites," *J. Vibroengineering*, vol. 14, no. 4, pp. 1852–1861, 2012.

[23] H. Stang, Z. Li, and S. Shah, "Pullout problem: stress versus fracture mechanical approach," *Journal of Engineering Mechanics*, vol. 116, no. 10, pp. 2136–2150, 1990.

[24] C. Y. Yue and W. L. Cheung, "Interfacial properties of fibrous composites," *Journal of Materials Science*, vol. 27, pp. 3173–3180, Jun 1992.

[25] A. E. Naaman, G. G. Namur, J. M. Alwan, and H. S. Najm, "Fiber pullout and bond slip. i: Analytical study," *Journal of Structural Engineering*, vol. 117, no. 9, pp. 2769–2790, 1991.

[26] A. Gent and G. Liu, "Pull-out and fragmentation in model fibre composites," *Journal of materials science*, vol. 26, no. 9, pp. 2467–2476, 1991.

[27] A. Gent and C. Shambarger, "Pull-out of short rods and fibres," *Journal of materials science*, vol. 29, no. 8, pp. 2107–2114, 1994.

[28] J. K. Knowles, "The finite anti-plane shear field near the tip of a crack for a class of incompressible elastic solids," *International Journal of Fracture*, vol. 13, no. 5, pp. 611–639, 1977.

[29] K. Rajagopal and L. Tao, "On an inhomogeneous deformation of a generalized neo-hookean material," *Journal of elasticity*, vol. 28, no. 2, pp. 165–184, 1992.

[30] J. Zhang and K. Rajagopal, "Some inhomogeneous motions and deformations within the context of a non-linear elastic solid," *International journal of engineering science*, vol. 30, no. 7, pp. 919–938, 1992.

[31] L. Tao, K. Rajagopal, and A. Wineman, "Circular shearing and torsion of generalized neo-hookean materials," *IMA journal of applied mathematics*, vol. 48, no. 1, pp. 23–37, 1992.

[32] K. Rajagopal, "A note on unsteady inhomogeneous extensions of a class of neo-hookean elastic solids," in *Mathematical Proceedings of the Royal Irish Academy*, pp. 47–57, JSTOR, 2004.

[33] C. Benjamin, M. Myneni, A. Muliana, and K. Rajagopal, "Motion of a finite composite cylindrical annulus comprised of nonlinear elastic solids subject to periodic shear," *International Journal of Non-Linear Mechanics*, 2019.